2019

Energy Transfer Between Eu2+ and Mn2+ for Na(Sr,Ba)PO4 and Ba2Mg(BO3)2

Kevin Bertschinger
Michigan Technological University, kbertsch@mtu.edu

ENERGY TRANSFER BETWEEN EU^{2+} AND MN^{2+} FOR $NA(SR, BA)PO_4$ AND $BA_2MG(BO_3)_2$

By

Kevin Bertschinger

A THESIS

Submitted in partial fulfillment of the requirements for the degree of

MASTER OF SCIENCE

In Applied Physics

MICHIGAN TECHNOLOGICAL UNIVERSITY

2019

This thesis has been approved in partial fulfillment of the requirements for the Degree of MASTER OF SCIENCE in Applied Physics.

Department of Physics

Thesis Advisor: *Dr. Jae Yong Suh*

Committee Member: *Dr. Jacek Borysow*

Committee Member: *Dr. Patricia Heiden*

Department Chair: *Dr. Ravi Pandey*

Contents

List of Figures

List of Tables

List of Abbreviations

ACL	Access Control List
AD	Avalanche Diodes
ADC	Analog to Digital Converter
CFD	Constant Fraction Discriminator
ET	Energy Transfer
LED	Light Emitting Diode
MCP	Microchannel plate
MCS	Multichannel Scaler
PL	Photoluminescence
PMT	Photomultiplier Tube
REI	Rare Earth Ion
SPAD	Single Photon Avalanche Diode
SPCM	Single Photon Counting Module
TAC	Time to Amplitude Converter
TCSPC	Time correlated single photon counting
TRPL	Time Resolved photoluminescence
XPS	X-ray Photoelectron Spectroscopy

Abstract

There is no debate of the affect that solid-state lighting has had on the world we live in. Throughout the centuries, lighting has continued to improve from kerosene lanterns to white light LEDs. Even though lighting today is sufficient there is still much room to improve color rendering index and efficiency. An active area of research to improve today's lighting technology is by doping inorganic phosphors with luminescent ion centers. There have been numerous reports of inorganic phosphors showing a variety of emission color and luminescence. In this thesis we discuss two new inorganic phosphors codoped with Eu^{2+} and $Mn^{2+}$and the energy transfer mechanism between the two. The phosphor $Na(Sr, Ba)PO_4$shows dual emission peaks with Eu^{2+} emitting blue light, and Mn^{2+} emitting red-orange light. In comparison, the phosphor $Ba_2Mg(BO_3)_2$ shows an overlapped emission from both Eu^{2+} and Mn^{2+} in the red-orange region. Energy transfer can occur when there is spectral overlap between the emission of $Eu^{2+}$and the absorption of Mn^{2+}. In this study, we compared the energy transfer when emission of Eu^{2+} is Stokes-shifted by the host material to an overlapping region of Mn^{2+} emission as seen in $Ba_2Mg(BO_3)_2$. With photoluminescence and time resolved photoluminescence measurements, we characterized the effects of the host material on the luminescence centers and the energy transfer mechanism. The data clearly suggests that the energy transfer efficiency increases for a specific overlap between the energy levels as seen in $Ba_2Mg(BO_3)_2$, compared to the greater

overlap seen in $Na(Sr, Ba)PO_4$.

Chapter 1

Introduction and Background Information

1.1 Introduction

Lighting efficiency was greatly improved with the white light emitting diode (LED). The Nobel prize was awarded for the discovery of the blue LED which enable white light LED [1]. There is still room to improve lighting by finding cheap, efficient, and improved light sources. Phosphors are material that have luminescence, and inorganic phosphors doped with luminescence materials has been an active area of research. There have been a variety of phosphors reported by combining different luminescence ions and different inorganic crystal structures to host. There is interest

in finding efficient phosphors that emit red light, and single component white light emitting phosphors. Luminescence ions that can convert from UV excitation to visible are desirable because these phosphors can be excited through a blue LED chip which essentially makes electrically driven visible light. Luminescence ions that serve well for improve white light through blue LED excitation is Eu^{2+} and Mn^{2+}. The Transition ion Mn^{2+} is important for phosphors because of the emission wavelength is in the green to red orange region depending on the hosting material. It is well known that Mn^{2+} has poor luminescence because the radiative transition is forbidden [2]. However, through an energy transfer mechanism Eu^{2+} which undergoes an allowed transition can greatly improved the luminescence of Mn^{2+}. In addition, with combination of Eu^{2+} and Mn^{2+} a single component and possible tunable lighting source can be created by codoping an inorganic hosting material. The combination of Eu^{2+} and Mn^{2+} is an almost magical combination for UV excited LED for future lighting applications. We report two new phosphors codoped with Eu^{2+} and Mn^{2+} which are $Na(Sr, Ba)PO_4$ and $Ba_2Mg(BO_3)_2$. Through photoluminescence (PL) the luminescence properties of Eu^{2+} and Mn^{2+} were studied. Time Resolved photoluminescence (TRPL) was used to verify and study the energy transfer mechanism in the different hosting materials. In conclusion, we find the ET process in $Ba_2Mg(BO_3)_2$ to be superior to the ET found in $Na(Sr, Ba)PO_4$ due to the difference in spectral overlap. The emission of Eu^{2+} overlaps with several higher energy absorption transitions of Mn^{2+} before Mn^{2+} emits light from the first excited state and the ground

state in $Na(Sr, Ba)PO_4$. while in $Ba_2Mg(BO_3)_2$ the emission of Eu^{2+} overlaps with the transition between the first excited state and ground state of Mn^{2+}only.

We begin with a discussion on the key component for inorganic phosphors: luminescence sources and hosting material. Followed by a brief introduction to optical processes and radiative transitions. We then discuss some background information pertinent to inorganic phosphors, and derive the energy transfer process. In chapter 2 we discuss the experimental techniques used to characterize phosphors with photoluminescence and time resolved photoluminescence. Then in chapter 3 we will review some current synthesized inorganic phosphors. Finally we present and discuss the main results of our studied phosphors $Na(Sr, Ba)PO_4$ and $Ba_2Mg(BO_3)_2$. Concluding remarks are made in Chapter 5.

1.2 Activators and Hosting material

To make a inorganic phosphor we need two ingredients. Luminescence source that will work to emit light, and a material to hold the luminescence source. The luminescence sources are called activators, and are typically rare earth ions or transition metals. The hosting material is some inorganic crystal structure.

1.2.1 Hosting Materials

The hosting material contains the luminescence centers, and plays an important role since it has an effect on the luminescence ions doped inside. Some examples of host materials will be discussed in more detail in chapter 2. Some common host materials are silicate, garnet, and nitride based inorganic materials. There is also a variety of crystal structures.

1.2.2 Activators

Activators are defects or impurities in a crystal host structure. Defects can take the form as nitrogen vacancy center in diamond which is a nitrogen atom in the crystal which has interesting luminescence properties. Impurities can be introduced into a crystal through different methods. Typically different crystal hosting materials are rare earth ions or transition metals as the impurities [3].

Impurities interact with the phonons in the crystal resulting vibronic system through electron-phonon interaction. Vibronic are continuous spectrum bands resulting from electronic states interacting with the continuous phonon modes of the crystal. The hosting crystal thus has a strong effect on the optical properties of the impurities. In addition, the crystal cations can interact with the orbitals of the

activators altering the luminescence properties of the activator.

1.2.2.1 Rare Earth Ions

Rare earth ions (REI) are known as the Lanthanides, and occur on the periodic table after Lanthanum element for the atomic numbers 57 to 71. REI's typically come in trivalent form with 3+ ionization or divalent form with 2+ ionization. REI's valence electrons are in the $4f$ orbital, and become ionized when losing electrons in the outer $6s^2$ orbital for the divalent form. REI's will turn into the trivalent form when losing electrons in the $4f$ orbital. For example, Eu has the electron configuration $[Xe]4f^7 6s^2$, and become the divalent form Eu^{2+} with electron configuration $[Xe]4f^7$. Likewise Eu will become the trivalent form Eu^{3+} by losing one electron in the outer $4f$ orbital to have the electron configuration $[Xe]4f^6$ [3]. The trivalent form is shielded by $5s$ and $5p$ outer electrons, so it is uncommon to see spectroscopic properties change from the hosting lattice. The divalent form can show change from the host lattice, and a variety of emission wavelengths have been reported for Eu^{2+} in different hosting materials. The transition states of the trivalent form can be summarize in Dieke diagram. Lastly the trivalent REI's are transition is parity spin forbidden, but the divalent REI have allowed transition [2].

1.2.2.2 Transition Metals

The 9 elements with atomic numbers from 21 to 30, and transition metals have electron configuration of the form $[Ar]3d^n4s^2$. These metals become divalent by losing electrons in the $4s$ orbital, and become trivalent by losing electrons in the d orbital. Strong coupling between transition metals and the hosting material exist because of the large radius of the $3d$ orbital. A good example of the hosting material effect is Cr^{3+} doped in Al_2O_3 and $Be_3AL2Si_6O_{18}$. When Cr^{3+} is doped in Al_2O_3 the ion emits red light, and when Cr^{3+} is doped in $Be_3AL2Si_6O_{18}$ the ion emits green light. The shift in wavelength is caused by the interaction from the crystal lattice and the transition metal [3].

1.3 Radiative Transition

1.3.1 Einstein Coefficients and Radiative Transitions

Einstein coefficient are an elegant way to described the radiative transition process that can occur in materials. Rate equations were first introduced by Albert Einstein to described quantum radiative transitions [4] in response to the work of Max Planck's distribution of thermal radiation [5]. The theory introduces three rate equations to described processes of absorption, spontaneous emission, and stimulated emission for

a material with Einstein coefficient quantifying each process (figure 1.1).

We will introduce rate equations with a simple two state system with $|1\rangle$ as state 1 and $|2\rangle$ as state 2. Imagine a photon will interact with the outermost electron of an atom, and when it does the electron will go from the lower energy state $|1\rangle$ to the higher energy state $|2\rangle$. This process is called absorption, and we can describe this process with the rate equation

$$\frac{dN_1}{dt} = -B_{12}N_1u(\omega) \tag{1.1}$$

with N_1 as the number of atoms in the lower energy state $|1\rangle$, B_{12} as the Einstein coefficient for absorption, and $u(\omega)$ as the spectral energy density. There are two radiative processes that an atom can undergo from $|2\rangle$ to $|1\rangle$ which are spontaneous emission and stimulated emission. Spontaneous emission is described by the rate equation

$$\frac{dN_2}{dt} = -A_{21}N_2 \tag{1.2}$$

with N_2 as the number of atoms in the energy state $|2\rangle$, and A_{21} as the Einstein coefficient for spontaneous emission. It is easy to see that equation 1.2 has the solution $N_2(t) = N_2(0)e^{\frac{-t}{\tau}}$ which means $A_{21} = \frac{1}{\tau}$ with τ as the lifetime of an emitter in the higher energy state. The lifetime τ of an emitter is an important quantity in the study of phosphors since a reduction in the lifetime alludes to nonradiative interactions in the host material. We will look at the reduction of lifetimes to characterize the energy

transfer process later. Stimulated emission is given by

$$\frac{dN_2}{dt} = -B_{21}N_2u(\omega) \tag{1.3}$$

with B_{21} as the Einstein coefficient for stimulated emission. In order for the rate equations to be consistent with Plank's blackbody radiation it is necessary that the Einstein coefficients are related to each other. It can be shown that

$$A_{21} = \frac{\hbar\omega^3}{\pi c^3}B_{21}$$

and

$$g_1B_{12} = g_2B_{21}$$

with g_1 being the degeneracy for state $|1\rangle$ and g_2 being the degeneracy of state $|2\rangle$[6].

With the three rate equations we can describe the radiative processes found for emitters. For the analysis of phosphors we are most interested in absorption and spontaneous emission. For new luminescence materials we are most interested in phosphors which absorb light in the UV region, and undergoes spontaneous emission in the visible region. The radiative lifetime τ is most important in this study, and as we will discuss in the next section. Laslty, We can draw information about the dipole moment of the emitter, and other interactions based on this value.

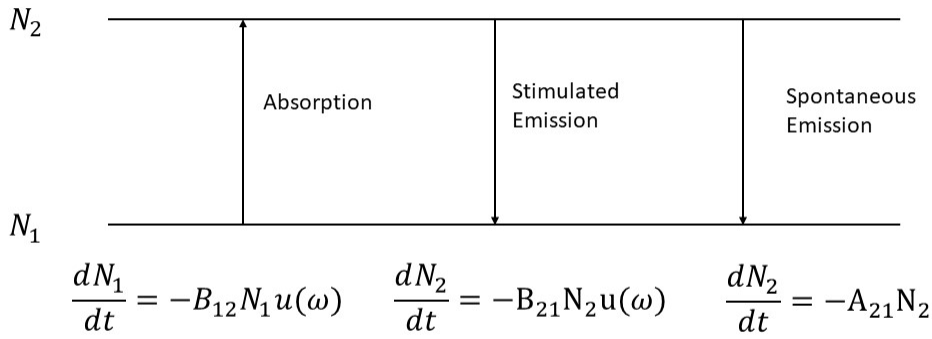

Figure 1.1: The process of absorption, stimulated emission and Spontaneous emission for a two level system

1.3.2 Fermi Golden Rule

Radiative transition can be described using quantum mechanics with Fermi Golden rule. Fermi Golden rule is derived using time dependant perturbation theory [7], and is stated as

$$\Gamma_{i-j} = \frac{2\pi}{\hbar}|M_{ij}|^2 g(\hbar\omega) \tag{1.4}$$

with a transition from state i to j, $g(\hbar\omega)$ as the density of states, and M_{ij} as a matrix element. The matrix element $|M_{ij}| = \langle i|H'|j\rangle = \int \psi_j^* H' \psi_i d^3\mathbf{r}$ with H' as the

perturbed Hamiltonian and $H' = -\mathbf{p} \cdot \boldsymbol{\xi_0}$ with $\mathbf{p}$ as a dipole of an atom and $\boldsymbol{\xi_0}$ as the electric field amplitude of light. The dipole of the atom is given by $\mathbf{p} = -e\mathbf{r}$, and we can rewrite $H' = e(x\xi_x + y\xi_y + z\xi_z)$ We can express the matrix element M_{ij} each polarization vector to obtain

$$M_{ij} = e\xi_x \int \psi_j^* x \psi_i d^3\mathbf{r} + e\xi_y \int \psi_j^* y \psi_i d^3\mathbf{r} + e\xi_z \int \psi_j^* z \psi_i d^3\mathbf{r}$$

$$= \boldsymbol{\mu_{ij}} \cdot \boldsymbol{\xi_0}$$

with the dipole moment given by $\boldsymbol{\mu_{ij}} = -e(\langle i|x|j\rangle + \langle i|y|j\rangle + \langle i|z|j\rangle)$. It can be shown through quantum mechanics that the dipole moment related to the Einstein coefficients with

$$B_{12} = \frac{\pi}{3\epsilon_0\hbar}|\mu_{12}|^2$$

and

$$A_{21} = \frac{\omega^3}{3\pi\epsilon_0\hbar c^3}\mu_{12}$$

. In conclusion, the density of states the dipole moment $\boldsymbol{\mu_{ij}}$ determines the transition rate for a electric dipole process [6]. The transition rate also depends on the states that the emitter energy level will transition. This leads to selection rules which we will discuss in the next section.

1.3.3 Selection Rules

Fermi Golden rule can be interpreted in terms of electric dipole selection rules since the matrix element equals $\mu_{\mathbf{ij}} \cdot \xi_{\mathbf{0}}$. The matrix elements depends on the initial and final quantum state of the emitter. If the selection rules are obeyed than there is a high probability of transition and the transition is allowed. If the selections rules are not obeyed than the transition probability is low and the transition is forbidden. We can describe selection rule in terms of a many electron system quantum numbers L, S, and J.The number L is the total angular momentum with Σl_i with l as the orbital angular momentum, S is the total spin with Σs_i with s as the spin, and J as the total total angular momentum with $J = \sqrt{L+S}$. The selection rules for electric dipole transitions are then $\Delta l = \pm 1$ $\Delta L = 0, \pm 1$, but $L = 0$ is forbidden. $\Delta J = 0, \pm 1$, but $J = 0$ is forbidden, and $\Delta S = 0$. The selection rules follow from parity of dipole operator, and can be different for different dipole types. For example magnetic dipole and electric quadrupole transition can take place for states of the same parity [6].

1.3.4 Fluorescence and Phosphorescence

Selections rules indicates allowed and forbidden transitions. Allowed transitions which obey electric dipole selection rules have a high probability of decaying into the lower energy state. This means a species can have a short radiative lifetime when excited

to the higher energy state known as fluorescence. When selection rules leads to a forbidden transitions the probability of decaying to the lower energy state becomes much less, and this leads to long radiative lifetimes known as phosphorescence [6] .

1.4 Non radiative Processes

Besides emission of a photon there are several processes an emitter can undergo to transition to a lower energy state. For the most part nonradiative transitions are undesirable. In this section we will mention a few common process that reduce the emission efficiency which are: multiphonon, luminescence quenching, and energy transfer.

1.4.1 Multiphonon

Phonon interaction is the main deexcitation process that competes with radiative emission. phonons are lattice vibrations in the crystal structure. When activators are placed in a crystal structure the outer electron will couple to the phonons creating a eletron-lattice coupling. When an emitter is promoted to higher energy state energy will be transferred to phonon lattice in the hosting crystal [8]. This interaction is also responsible for stokes shifting and broadening the emission of the activators, and is illutrated in figure 1.2.When absorption occurs the activator will be promoted

to a higher energy state from A to B. Then the emitter will undergo multiphonon deexcitation through C towards the lower energy level in the potential well. If there is overlap between the potential well of the lower energy state then the activator will undergo multiphonon radiation to the lower energy state only (figure 1.2 (b)). If the potential well of the lower energy does not overlap with the energy levels of the activator then after undergoing multiphonon radiation C the activator will then radiative photons D to reach the lowest energy state [2].

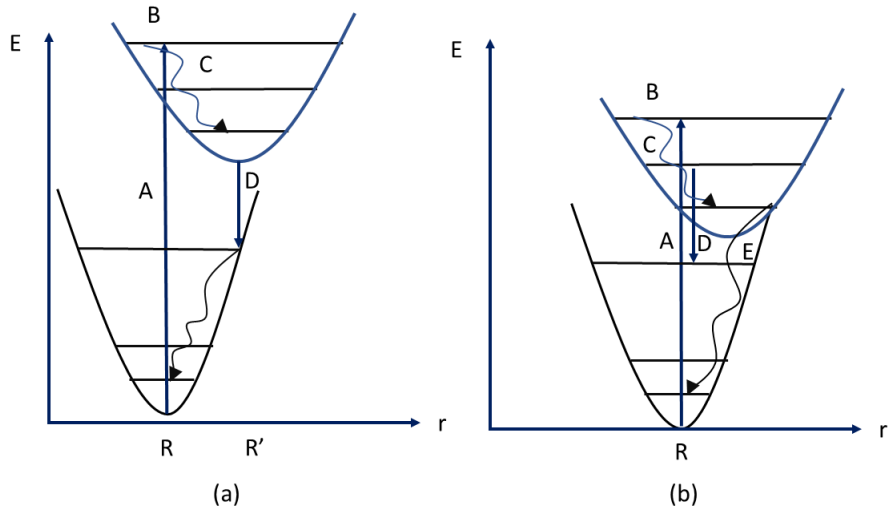

Figure 1.2: Through eletronc-lattice coupling the energy levels form parabolic energy wells. The coupling can cause the energy levels to be stoke shifted and energy will deexcite in the form of phonons or lattice vibrations. (a) Shows phonon deexication along with radiative emission. (b) shows only phonon deexcitation due to the overlap in potential wells and energy diagram of activator

1.4.2 Luminescence Quenching

There are processes which an cause the luminescence to decrease known as quenching. Quenching is caused by reaching a critical concentration of activators in a host material or from thermal interaction.

1.4.3 Thermal Quenching

Luminescence can be effected by the temperature which can result in luminescence quenching. This process can be described using configuration coordinates that were used to described mulitphonon nonradiative process (figure 1.2). In the case of thermal quenching the emitter will go to the higher energy state through absorption, and will relax into the lower energy state of a parabolic well of the higher energy state through a mechanism such a mulitphonon. Then it will be thermally activated to a higher state in the excited parabolic well. When the energy increases to a point were the parabolic well of of the higher energy state crosses with the parabolic well of the lower energy states the system will relax to the ground state through nonradiative process such a mulitphonon. You can think as thermal quenching as perturbing the a particle on parabolic well to a higher energy that will overlap with the lower parabolic

well. This probability of thermally activated dexicatation can be described by

$$W_{NR} = sexp(\frac{-\Delta E_{tq}}{k_B T})$$

with $-\Delta E_{tq}$ as the activation energy for thermal quenching, and s is the frequency factor. The quantity ΔE_{tq} is the energy different between the lower energy state in the higher parabolic well, and the energy when the system is excited to a higher energy in the well such that it overlaps with the lower parabolic well[8].

1.4.3.1 Concentration Quenching

Increasing the number of activators will cause the luminescence to increase due to the increase in the absorption coefficient. However, as the concentration increases to a critical concentration it is not uncommon to observe quenching in the luminescence which is known as concentration quenching. Concentration quenching can be described by two different mechanism which are donor-killer and cross-relaxation. For donor-killer, the activator will transfer energy to other activators of the same kind. This process will occur throughout a chain of activators until the energy is loss to a nonradiative process. The emitter that loses the energy through a nonradiative process is called a killer or donor sink. For cross relaxation, the energy is loss through a resonance energy transfer process between two activators. Cross relaxation will occur due to the level structure of an emitter. This results in the transfer from high energy

levels to lower energy levels of the other emitter. This will result in quenching for luminescence associated with higher energy levels of the emitter, and enhanced emission of luminescence for lower energy levels of the emitter. Concentration quenching can be deduced by measuring the lifetime of activators. A reduction in lifetime indicates energy transfer process which is the basis for a quenching process to occur [2].

1.4.4 Energy Transfer

Energy transfer is an important process for the development of single component phosphors. In this section we will derive and explain the energy transfer process. First we will derive energy transfer between two particles with classical electrodynamics to build an intuition for the type of interaction that can occur (figure 1.3). We will assume two particles A and B with charge densities $\rho_A(\mathbf{r}')$ and $\rho(\mathbf{r}'')$ with $\mathbf{r_A}$ the distance to particle A and $\mathbf{r_B}$ the distance to particle B. The distance to the charge density of each particle is given by r' for particle A, and r'' for particle B. We will also assume the charge distribution of each particle is much smaller than the distance between the particles so we can make a multipole expansion. Lastly we will assume that the energy transfer occurs from one particle to the other. We will called the particle that gives its energy away as the donor, and the particle that receive the energy the acceptor. This assumption is justified because the donor particle emission wavelength will overlap with the absorption of the acceptor. Typically it is not

possible for the acceptor particle to give energy to the donor since there is no overlap between the emission of the acceptor and absorption the donor.

We can write the coulomb interactions as

$$V_{AB} = \frac{1}{4\pi\epsilon_0} \int\int \frac{\rho_A(\mathbf{r}')\rho_B(\mathbf{r}'')}{|\mathbf{r}' - \mathbf{r}''|} d^3r' d^3r'' \tag{1.5}$$

Now we can take the multipole expansion to obtain

$$V_{AB} = \frac{1}{4\pi\epsilon_0}[\frac{q_A q_B}{R} + \frac{q_A \mu_\mathbf{B} \cdot \mathbf{R}}{R^3} - \frac{q_A \mu_\mathbf{A} \cdot \mathbf{R}}{R^3} + \frac{R^2 \mu_\mathbf{A} \cdot \mu_\mathbf{B} - 3(\mu_\mathbf{A} \cdot \mathbf{R})(\mu_\mathbf{B} \cdot \mathbf{R})}{R^5} + \dots] \tag{1.6}$$

with

$$q_i = \int \rho_i(\mathbf{r}) d^3r'$$

$$\mu_\mathbf{i} = \int \rho_i(\mathbf{r})(\mathbf{r}' - \mathbf{r}'_\mathbf{i}) d^3r'$$

and

$$Q_i = \int \rho_i(\mathbf{r}') \frac{1}{2}[(\mathbf{r}' - \mathbf{r}'_\mathbf{i})(\mathbf{r}' - \mathbf{r}'_\mathbf{i}) - \frac{I}{3}|\mathbf{r}' - \mathbf{r}'_\mathbf{i}|^2] d^3r'$$

The first term $\frac{q_A q_B}{R}$ in equation 1.6 is charge-charge interactions, the second third term $\frac{q_i \mu_\mathbf{j} \cdot \mathbf{R}}{R^3}$ is charge-dipole, and the last term $\frac{R^2 \mu_\mathbf{A} \cdot \mu_\mathbf{B} - 3(\mu_\mathbf{A} \cdot \mathbf{R})(\mu_\mathbf{B} \cdot \mathbf{R})}{R^5}$ is dipole-dipole interaction. Higher order terms continue in the expansion to include dipole-quadrupole and quadrupole-quadrupole interactions. The above derivation emphasizes that the interaction between the two particles will take the form between two various dipole

moments. Now we will build upon our model for two interacting particles using a

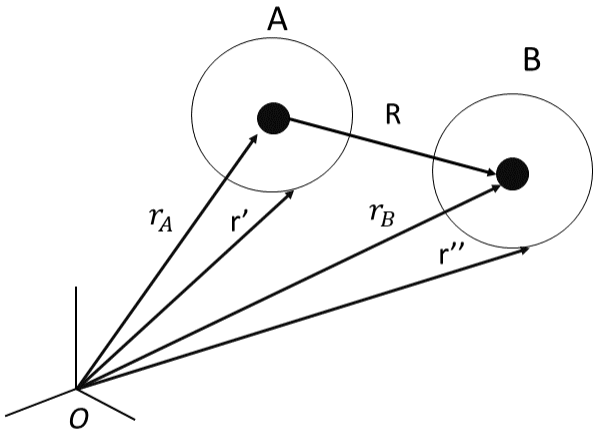

Figure 1.3: Diagram for two particles interacting. r_A points to particle A and r' points to the charge distribution of particle A, r_B points to particle B, r'' points to the charge distribution of particle B, and R points from particle A to particle B.

semi classical approach. We can calculate the energy transfer between two particles by looking at the transfer between two discrete energy levels. We can look at the transfer rate from donor to acceptor present as $\gamma_{D\to A}$ and decay rate without the acceptor present as γ_0. We can then write

$$\frac{\gamma_{D\to A}}{\gamma_0} = \frac{P_{D\to A}}{P_0} \tag{1.7}$$

with $P_{D\to A}$ as the donor energy per unit time absorbed by acceptor, and P_0

as the average power of a radiating dipole and has units of energy/time. This can be given as

$$P_0 = \frac{\mu_D^2 n(\omega_0)}{12\pi\epsilon_0 c^3}\omega_0^4$$

with μ_D as the dipole moment of the donor, $n(\omega_0)$ as the index of refraction, and ω_0 as the absorption frequency of the acceptor and emission of the donor. We can calculated the energy transfer from the Poynting vector as

$$P_{D\to A} = -\frac{1}{2}\int Re\{\mathbf{j_A^*}\cdot\mathbf{E_D}\}d^3r$$

with the current density described the the dipole approximation $j_A = -i\omega_0\mu_\mathbf{A}\delta(\mathbf{r}-\mathbf{r})$. $P_{D\to A}$ can be reduced to

$$P_{D\to A} = \frac{\omega_0}{2}Im\{\mu_\mathbf{A}^*\cdot\mathbf{E_D}(\mathbf{r_A})\}$$

The acceptor is then a transition dipole moment described by

$$\mu_A = \overleftrightarrow{\alpha}E_D(r_A)$$

The polarization tensor which we can define as $\overleftrightarrow{\alpha} = \alpha_A\mathbf{n_A}\mathbf{n_A}$. We can now write

$$P_{D\to A} = \frac{\omega_0}{2}Im\{\alpha_A\}|[\mathbf{n_A}\cdot\mathbf{E_D}(\mathbf{r_A})|^2 \tag{1.8}$$

Note that the imaginary part of the polarization is the energy absorption, $\mu_{\mathbf{A}}$ is an induced dipole, and the absorption rate scales with the square of the E-field. Now we will express the polarizability in terms of the absorption cross section with

$$\sigma(\omega) = \frac{< p(\omega) >}{I(\omega)}$$

with $< p(\omega) >$ as the average absorption over all dipole orientations for the acceptor, and $I(\omega)$ as the incident intensity. It then follows that

$$\sigma(\omega_0) = \frac{(\omega_0/2) Im\{\alpha(\omega_0)\} < |\mathbf{n_p} \cdot \mathbf{E_D}|^2 >}{\frac{1}{2}(\epsilon_0/\mu_0)^{\frac{1}{2}} n(\omega_0)|E_D|^2}$$

$$= \frac{\omega_0}{3}\sqrt{\frac{\mu_0}{\epsilon_0}}\frac{Im(\alpha(\omega_0))}{n(\omega)}$$

We can simplify this expression further by by taking orientation dipole average with

$$< |\mathbf{n_p} \cdot \mathbf{E_p}|^2 >= \frac{|E_p|^2}{4\pi}\int_0^{2\pi}\int_0^{\pi}[\cos(\theta)]\sin(\theta)d\theta d\phi = \frac{1}{3}|E_p|^2$$

We can then write equation 1.6 as

$$P_{D\to A} = \frac{3}{2}\sqrt{\frac{\epsilon_0}{\mu_0}} n(\omega_0)\sigma_A(\omega_0)|\mathbf{n_n} \cdot \mathbf{E_D}(\mathbf{r_A})|^2 \tag{1.9}$$

Now lets rewrite the donor field $\mathbf{E_D}$ in terms of a free space green function as

$$\mathbf{E_D} = \omega_0^2 \mu_0 G(\mathbf{r_D}, \mathbf{r_A}) \mu_D \mathbf{n_D} \tag{1.10}$$

We can combine equation 1.9, P_0, and 1.10 to obtain

$$\frac{\gamma_{D\to A}}{\gamma_0} = \frac{\frac{3}{2}\sqrt{\frac{\epsilon_0}{\mu_0}} n(\omega_0)\sigma_A(\omega_0)|\mathbf{n_n}\cdot\mathbf{E_D}(\mathbf{r_A})|^2}{\frac{\mu_D^2 n(\omega_0)}{12\pi\epsilon_0 c^3}\omega_0^4}$$

$$= \frac{\frac{3}{2}\sqrt{\frac{\epsilon_0}{\mu_0}} n(\omega_0)\sigma_A(\omega_0)|\mathbf{n_n}\cdot\mathbf{E_D}(\mathbf{r_A})|^2 12\pi\epsilon c^3}{\mu_D^2 n(\omega_0)\omega_0^4}$$

We can cancel terms, and express the electric field of the donor in terms of a Green function to obtain

$$= 18\sigma_A(\omega_0)\pi\epsilon_0 c^3 \mu_0^2 \sqrt{\frac{\epsilon_0}{\mu_0}} |\mathbf{n_A}\cdot G(\mathbf{r_D}, \mathbf{r_A})\cdot\mathbf{n_D}|^2$$

We can add several terms, and noticed that $\epsilon_0\mu_0^2\sqrt{\frac{\epsilon_0}{\mu_0}}c^3 = 1$ to obtain

$$= \frac{9c^4}{8\pi R^6}\frac{\sigma_A(\omega_0)}{n(\omega_0)^4\omega_0^4}\{16\pi^2 k^4 |\mathbf{n_A}\cdot G(\mathbf{r_D}, \mathbf{r_A})\cdot\mathbf{n_D}|^2\}$$

with $k = \frac{w_0 n}{c}$

we can define the function $T(\omega_0) = 16\pi^2 k^4 |\mathbf{n_A}\cdot G(\mathbf{r_D}, \mathbf{r_A})\cdot\mathbf{n_D}|^2$ to obtain a simpler expression

$$\frac{\gamma_{D\to A}}{\gamma_0} = \frac{9c^4}{8\pi R^6}\frac{\sigma_A(\omega_0)}{n(\omega_0)^4\omega_0^4}T(\omega_0) \tag{1.11}$$

From equation 1.11 we can see that the energy transfer rate it proportional to the absorption cross section, $\frac{1}{R^6}$ and the function $T(\omega)$. Recall that the $T(\omega)$ depends on the green function G which is proportional to the electric potential of the system which we can express in terms of the dipole-moment interaction. When characterizing the energy transfer rate the overlap between the emission of the donor and absorption of the acceptor, the distance between the two particles, and dipole moment interaction [9].

1.5 Effect of Hosting Material on Activators

The optical properties of an emitter can be altered by the host material. The photoluminescence properties can be effected by the host crystal in two ways: the centroid shift and crystal field splitting (figure 1.4). These effects can cause a redshift in the emission by changing the energy difference.The d-d transition common among transition metals tends to be more effected by crystal effects while REI's are not. The centroid shift is linked to the polarizability of the surrounding anion which causes the interelectron repulsing to decrease. Crystal field splitting is the splitting of the energy levels of the activator ions, and is caused by interaction between the anion and

molecular orbitals. The activator ions in the d orbital hybridize creating bonding orbitals at lower energies and antibonding orbitals at higher energies. This bonding and antibonding do not always occur at the same amount, so crystal field splitting may either increase or decrease. It has been shown that Crystal field splitting is largest for octahedral coordination, then cubic, dodecahedral, and smallest for cuboctahedral [10].

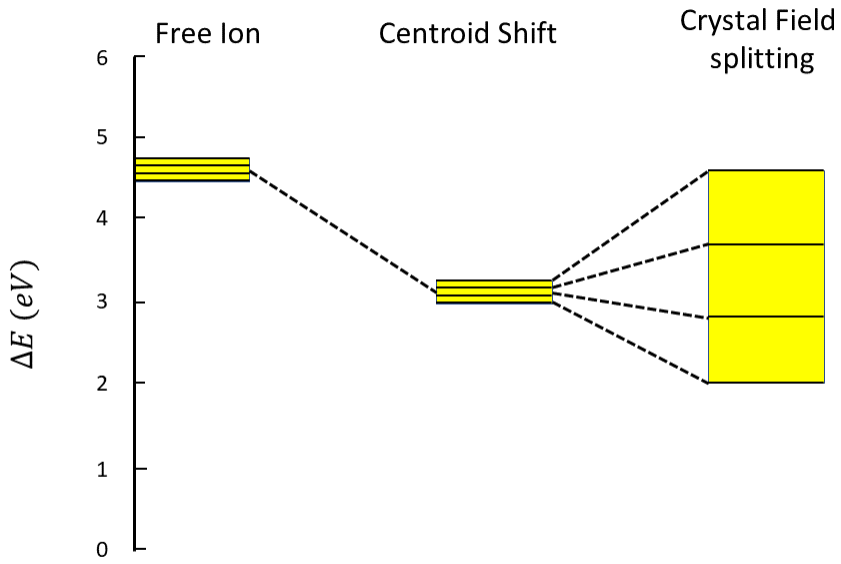

Figure 1.4: The effect the hosting material has on emitters. There is a centroid shift which shifts the energy levels. The Crystal field splitting causes the energy levels in the ion to split.

1.6 Chromaticity Scale

In the search for new luminescent materials it is important to compared the luminescence to how the human eye sees light. By combing three colors white light can be achieved [11]. The photopic vision is sees between 380 nm to 780 nm with the peak wavelength at 555 nm. The perception of light is given by the flux of light on the eye. The conversion efficiency of of light to a electrical impulse can e given by

$$\eta = \frac{\Phi}{P}$$

with Φ as the flux of light, P as the power consumed. We can re-express the conversion efficiency through

$$\eta = \frac{\Phi_e}{\Phi_e} = \frac{683lm}{w} \frac{\int V(\lambda)S(\lambda)d\lambda}{\int S(\lambda)d\lambda}$$

with $V(\lambda)$ as the luminescence efficiency function for the eye, and $S(\lambda)$ is the spectral power distribution function. The function $S(\lambda)$ can be described with a Gaussian function in the form

$$s(\lambda) = P\frac{1}{\sigma\sqrt{2\pi}} e^{\frac{-1}{2}\frac{(\lambda-\lambda_{peak})^2}{\sigma}}$$

with $\sigma = \frac{\lambda_{peak}^2}{2hc}\frac{E}{\sqrt{2\ln(2)}}$ We can introduce chromaticity coordinates and a coordinate scale to describe the color which will be seen by a person. The chromaticity coordinates are defined as

$$X = \int \bar{x} S(\lambda) d\lambda$$

$$Y = \int \bar{y} S(\lambda) d\lambda$$

$$Z = \int \bar{z} S(\lambda) d\lambda$$

The values of X, Y, and Z determines the colors lightness, hue, and saturation. The 1931 CIE chromaticity scale gives the color render by a combination of emissive sources (figure 1.5). The coordinates can be found from X, Y, and Z to see that color will be given for a color combination with

$$x = \frac{X}{X+Y+Z}$$

$$y = \frac{Y}{X+Y+Z}$$

$$z = \frac{Z}{X+Y+Z}$$

From these coordinates we can quantify the color that phosphors emit [8].

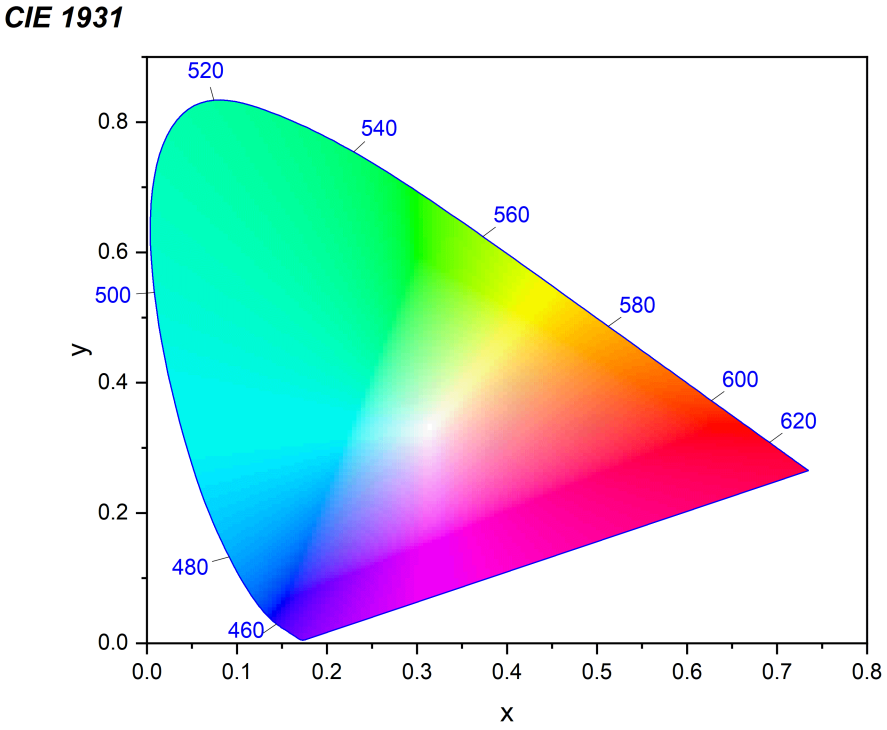

Figure 1.5: A CIE 1931 chromaticity Scale used to classify color index from a combination of emission wavelength of multiple wavelength

Chapter 2

Time Resolved Photoluminescence

A key figure of merit of phosphors for solid state lighting are the luminescence properties. We are interested in To characterize the activators in different host materials by looking at the luminescence. PL measurements are useful to determining luminescence, and TRPL is useful for determining the radiative lifetime of activators in phosphors.

2.1 Photoluminescence

PL is the emission of light after absorption a photon of a higher energy. This is useful for analyzing the emission spectrum of luminescence centers in different hosting materials. Typically phosphors absorbed light in the UV range, and emits light in the

visible range. For REI's and TM the emission wavelength depends radiative transition for the outer electrons. The crystal field of the host material can alter the emission intensity and the wavelength of the mission. We can also determine the color of the luminescence of the phosphor using the chromatically scale based on the PL.

To measure the emission for different concentrations we keep the PL constant along with the optical set up. This was done by keeping the repetition rate and the power output of the excitation laser the same. Misalignment will cause the emission to decrease, so it was necessary to ensure each measurement had the excitation laser on the sample at the focal point of the objective lens.

2.2 Time Resolved photoluminescence

We can further characterize activators by looking at the time resolved PL (TRPL). This process measures the PL as a function of time [3]. From this information we can determine the spontaneous emission rate of the activators, and characterize the effect of the hosting material on the activators. In addition, we can study the ET process in hosting materials which are codoped with two activators. In this section we will introduce the experimental method used to measure the radiative lifetime of activators. First we will explain time correlated single photon counting (TCSPC) method which is used to measure fluorescence lifetime. Than we will discuss each piece of equipment required for TCSPC before going in depth for the hardware that makes

TCSPC possible. We will discuss both traditional TCSPC components and modern TCSPC components. Lastly we will discuss measurements of phosphorescence decays which are much longer than fluorescence decays and make TCSPC unnecessary.

2.2.1 Time Correlated Single Photon Counting

TCSPC is a standard method for measuring fluorescence decays from emitters. TRPL can determine the spontaneous emission rate of the activators, and characterize the effect the hosting material has on the emitters. The TRPL can also be used to analyze energy transfer between two activators. After the activator has been excited by a laser pulse a certain amount of time will pass before the activator spontaneously emits the photon which will be detected by a single photon counting module (SPCM), and the time between excitation and emission will be recorded with a start-stop time fashion 2.1. The emission of the photon will be proportional to transition probability given by Fermi's golden rule 1.4 . The inverse of the transition probability gives the mean lifetime of the spontaneous emission $\gamma = \frac{1}{\Gamma_{i \rightarrow j}}$ [6]. This results in a series of events for different recorded start-stop times which is recorded in the form of histograms representing different time bins 2.2. A series of histograms for different recorded start-stop times will be recorded. The histogram series will decay exponentially in conjunction with the mean lifetime of the activator [12] .

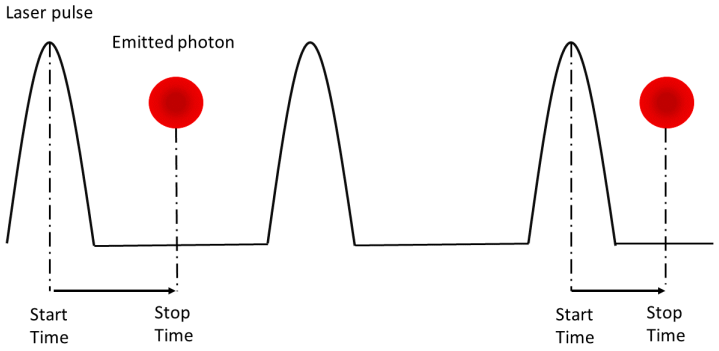

Figure 2.1: The measurement process between the excitation of a laser pulse and the emission of a photon. when the laser pulse is sent towards the phosphor the time is started, and when the photon is emitted the time is stopped.

2.2.1.1 Experimental Set up

The experimental set up consist of a pulse laser source, a monochromator, SPCM, and an event counter designed for TCSPC. The laser source is a 405 nm wavelength with adjustable repetition rate, and is directed towards a sample stage using a 405 nm dichroic mirror. The dichroic mirror reflects light at 405 nm and allows light outside that wavelength to transmit through the mirror. A 405 nm cut off filter is placed in the beam path before the emitted light is focused into the monochromator. The cut off filter blocks scattered laser light which will effect the timing in TCSPC. The emitted light is spectrally filtered to the desired wavelength using the monochromator since we are studying phosphors codoped with two different activator. We can spectrally filter the emission of the wavelength to study the activators individual in the case that the activators emit light at different wavelengths. After passing the light through the

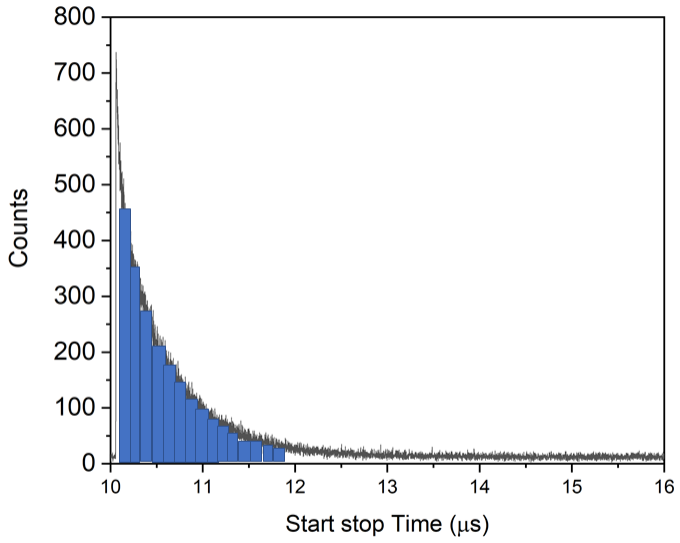

Figure 2.2: After the time difference is found for each start stop sequence. The time difference is then converted to a series of histograms. From the histograms we can infer an exponential decay of the fluorescence

monoochromator the light is directed towards a SPAD using a multimode fiber. The sync signal is sent to an event counter which is the Hydraharp 400 from the pulse laser driver, and the SPAD detected signal is sent to channel one of the Hydraharp 400. The decay curve is then acquired through the Hydraharp electronics and software. After a specific acquisition time a decay curve is obtained, and fitted using a single exponential function in OriginPro to obtain the mean radiative lifetime 2.3 [12].

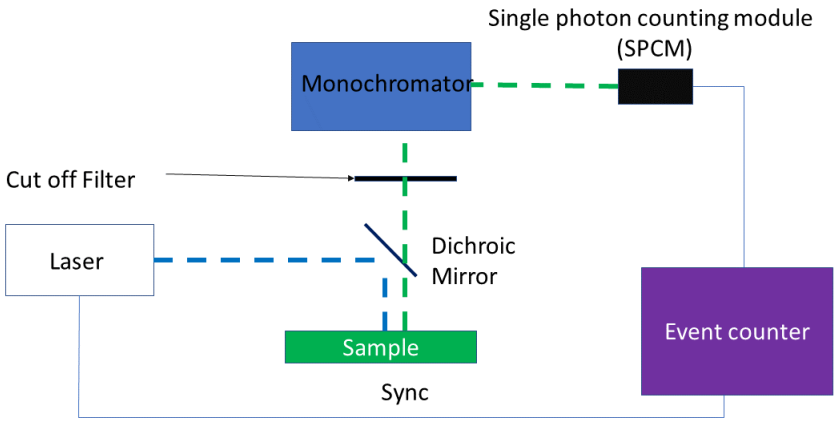

Figure 2.3: Experimental apparatus for measuring Time correlated single photon counting (TCSPC)

2.2.2 Equipment

2.2.2.1 Single Photon Detectors

A key piece of equipment for this method to work is a single photon counting device. It is possible to use photomultiplier tube (PMT), microchannel plate (MCP) or a single photon avalanche diode (SPAD). Several important quantities that are encounter in single photon detectors are dark count, dead time, timing jitter, and detection efficiency. Dark counts are the inevitable output pulse in the absence of a photon event caused by thermal effects. It is ideal to have low dark counts compared to the detection rate of photons. Dead time is the amount of time for the detector to register the detection of a photon. Dead time will cause the detector to fail to

register a photon event since the detector is still processing the previous detection. This will lead to an over representation of early photon events causing the measured fluorescence decay time to be shorter than the actual. This is known as pile up error.

A PMT is a photocathode tube that turns photon into electron that are directed towards a dynode. This dynode produces more electrons from the first electrons. This results in a multiplication effect for each electron, and this effect can be further amplified by adding series of dynodes until the signal is high enough to be detected by standard electronics [13]. An anode collects the electrons, and gives an output current which increases with the number of electrons . A PMT can convert a single photon to a detectable electronic pulse. The efficiency of a PMT ranges from 10 % to 40 %, and can have low dark counts and dead times. A limitation is the PMT is required to operate in a vacuum tube [13].

A MCP is is a channel with a high voltage applied across the channel walls. When a photon incidents upon the plate a electron is produced and when the electron bounces off the channel it produces a secondary electron. MCP can be placed in series to achieve high electrical signal from a single photon. MCP are typically between 3 μm to 10 μm [14].

A SPAD is a p-n junction diode that undergoes avalanche breakdown when a photon is incident on the device. A p-n junction is an n-type semiconductor connected to a p-type semiconducting crystal. A n-type semiconducting material is doped

with an electron donor element. A p-type semiconducting material is doped with an electron accepting element which is called a hole.The n-type can now conduct electricity with an unbound electron while the p-type does so with holes. Sandwiching a n-type material with a p-type material forms a p-n junction. When a battery source is connected to a p-n junction with the positive terminal on the p-type and negative terminal on the n-type terminal current will flow through the diode from electron hole recombination which is known as forward-biased. When the battery terminal is place in the opposite configuration with the negative terminal on the p-type and the positive terminal on the n-type and depletion region is formed at the interface of the n-type and p-type material. This is known as a reverse-bias and prevents current from flowing through the diode [15]. When a diode is reverse bias there exists above the breakdown voltage that will cause current between the two junctions which is know as avalanche breakdown. When an incident photon interacts with the p-n junction an electron hole pair is created which avalanches to create a current which is known an ionization impact. This process is highly sensitive to incoming photons, and will produce a strong detectable current pulse. The amount of time for the SPAD to fully process an event results in a dead time. The SPAD detector will trigger without the detection of a photon which results in the dead counts [14].

2.2.2.2 TCSPC Event Counter

The TCSPC event counter is a system formed by several building blocks creating a single integrated unit. There is a traditional TCSPC event counter, and a simplified modern TCSPC event counter. We will first discuss the traditional event counter to illustrate the different processes that are needed to improve the accuracy measure lifetimes (figure 2.4). Then we will discuss modern event counters which have simplified circuitry(figure 2.5).

The traditional TCSPC event counters consists of Constant fraction discriminator (CFD), level trigger, time to amplitude convertor (TAC), analog to digital convertor (ADC) and histogrammer (figure 2.4). The CFD is used to improved the precision of measurements taken from the detector. To obtain accurate time measurements it is necessary to obtain an accurate triggering of the photon. Electrical pulses created by the detection of a single photon suffer from amplitude jitter which would cause a timing jitter. In other words, there is variation in the pulse shaped and amplitude that is created by the single photon detection. Using a level trigger to set a standard threshold voltage to trigger will help reduce noise from setting off the timer, but the start time of the TCPSC system will suffer from inaccuracies due to the variation in the pulse shape. The CFD is used to improve the precision of the timing by triggering at a constant fraction of the pulse amplitude. A way to implement a CFD is by taking the difference in the original electrical pulse, and a delay pulse.

The zero cross point will be independent of the amplitude jitter providing accurate timing of the pulse [14]. A sync signal is required as a reference to determine the time of emission. The sync signal is usually a well defined pulse, so a level trigger can be used to removed any unwanted noise from detected sync. A level trigger sets a level which will trigger when the voltage reaches a specific threshold. The TAC is used to determine the time difference between the sync pulse and detected pulse after the CFD. The TAC is a linear ramp generator that is started by one signal and stop by the other. The TAC can be started by either using the detected signal or sync signal. The voltage is proportional to the time difference between the two signals [12]. The TAC signal is then sent to the ADC which needs to convert the voltage to a time signal with a short deadtime and linear signal.The histogrammer transfer the information from the ADC to histogram memory. This is done by fast digital logic field programmable gate arrays. The different histograms are then are then used to determine the decay time of the emission [12].

The Modern TCSPC set up can be simplified by combining the TAC and ADC into a single component called a time to digital converter (TDC). This can improve the timing resolution to picosecond range. TDC works by measuring the time difference through a delay of times of signals in semiconducting logic gates. One way to build a TDC is to construct a chains of logic gates. This can be used to determine the gate delay [14]. The TDC allows the building block TCSPC to be simplified 2.5. We can place CFD for both the sync input and the detector input

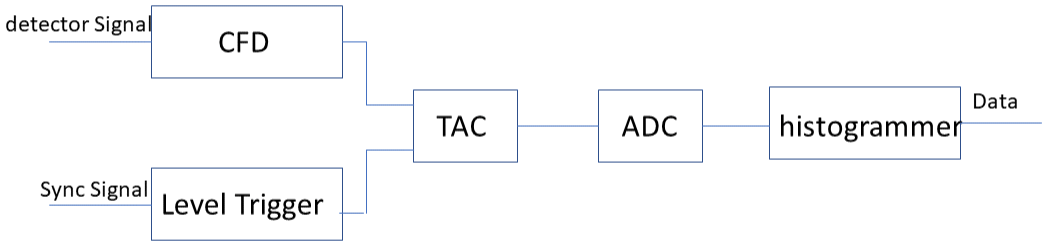

Figure 2.4: Building blocks for TCSPC

and then have a TDC for both signals to measure the time of each input. We then can subtract the time from the each TDC to obtain the time difference. The system works as a stopwatch with the sync signal as the start time, and the detected signal as the stop time. Each start-stop time is then converted to histogram data for each time bin, and this gives the decay curve of the fluorescent sample [12].

2.2.3 Monochromator

A monochromator is a mechanical device with the function to select a wavelength of light. A monochromator works by using diffraction on grating to separate the wavelengths of light through dispersion. The dispersion is caused by a diffraction

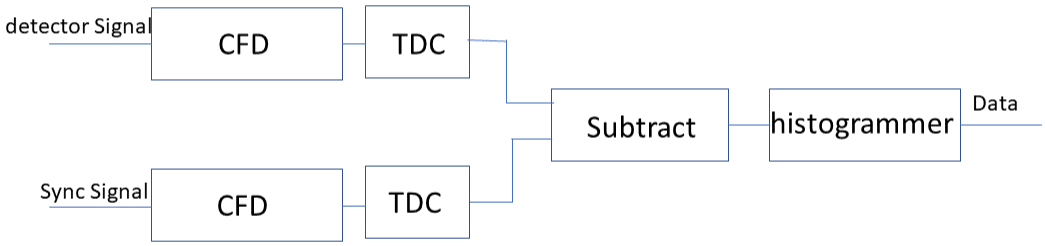

Figure 2.5: Building blocks for Modern TCSPC

grating which is a periodic structure with groove forming a sawtooth pattern. The pattern causes light at different wavelengths to be reflected at different angles.This will cause a beam of monochromatic light to separate, and by using a finite slit width we are able to select the desire wavelength of light. The output of light will have some linewidth, and the resolution that is obtainable depends on the slit width [2].

2.2.4 Phosphorescence Measurement

Phosphorescence is emission of radiation that occurs over a long period of time. Typically 100 μs to a few ms. To measure phosphorescence decay TCSPC is inefficient due to the long time scales. Also a single light pulse at a low repetition rate does

not provide an effective excitation due to the lower average power. Phosphorescence decays is associated with forbidden transitions, and take substantial time to fully emit [6]. To measure the phosphorescence decay, we make use of a multichannel scalar (MCS) instead of the Hydraharp 400. The MCS is able to record multiple photon counts per excitation signal. This allows the ability to excite the sample with a high excitation power, and counts the emission of photons over a period of time channels [16]. The phosphorescence measurement uses the same experimental set up as the TCSPC, we just replace the Hydraharp 400 with SR430 MCS, and use an optical chopper to create a high intensity periodic signal. The chopper can operate at a low frequency, so there is a high intensity excitation, and a long time period to allow the sample to fully emit light.

A MCS is similar to the event counter described above. The main difference is the MCS counts the number of photons for a given time window. For the experiment we used a SR430 from Stanford research. There is an input for a periodic excitation source and the detected signal. The time window is set by specifying the width of a time bin which can range from 5 ns to 10 ms. The periodic excitation will trigger the MCS to begin counting detected pulses from the detector within time bin windows. This is ideal for phosphorescence since after a substantial excitation period the MCS can count the emitted photons over a long time period [17].

The optical chopper is a mechanical device with a wheel that periodically blocks the excitation light. The blocking of the light is done with a wheel that has

an opening and blocking segments throughout the wheel. The wheel is spun at a specified frequency from a driver. For the phosphorescence measurements taken the wheel was spun at 20 Hz with a single opening segment in the wheel that is 1 cm across.

Chapter 3

Review of Phosphors doped with Rare Earth Ions

There is current interest in making new light sources. Doping inorganic phosphors with rare earth ions and transition metals is an active area of research. In this chapter we will discuss some research that has has already been done to give the reader some background. The goal is to find cheap, efficient, and improved light sources. Over the years there have been a variety of inorganic phosphors which have been doped with activators showing a variety color and luminescence properties. First, we will discuss some common phosphor families, then talk about a few codoped phosphors.

3.1 Phosphor Families

3.1.1 Garnet

Garnet structure can generally be written in the form $X_3Y_2Z_3O_{12}$ with X at eight fold coordinated cation, Y as the sixfold coordinated cation. Typically X has a divalent Ca, Mn, and Fe while Y is composed of Al, Fe, and Cr. The cubic garnet crystal structure is a member of the space group Ia-3d. There are several garnet structures such as $Y_3Al_5O_{12} : Ce^{3+}$ (YAG:Ce), $Ca_3Sc_2Si_3O_{12} : Ce^{+3}$, and $Lu_2Ca_Mg_2(Si, Ge)_3$ [8]. Yttrum-aluminum garnet doped with Ce^{+3} (YAG:Ce) is the most popular garnet due to yellow emission [10]. This garnet has a large crystal field splitting from Ce^{3+}, with excitation band at 340 nm and 460 nm. The excitation makes YAG:Ce an excellent phosphor for a blue LED chip. YAG:Ce has an broad emission peak 540nm which is yellowish, and when combined with the blue emission of InGaN it forms a whitish light [10]. The phosphor $Ca_3Sc_2Si_3O_{12} : Ce^{3+}$ is a silicate garnet with a cubic structure. The crystal field effects causes a shorter emission from the Ce^{2+} which makes $Ca_3Sc_2Si_3O_{12} : Ce^{3+}$ suitable as a green emitting phosphor. The phosphor $Lu_2CaMg_2(SiGe)O_{12} : Ce^{3+}$ has a smaller unit volume compared to the other two mention garnet based phosphors. This means the Ce^{+3} ion will be effected more by the Crystal field effects. The phosphor $Lu_2CaMg_2(SiGe)O_{12} : Ce^{3+}$ has a broad

excitation band at 470 nm and a red shifted emission beak at 605 nm.

3.1.2 Silicate

Silicate phophates can come in two forms: a a two part system with $MO - SiO_2$ with $M = Ca, Sr, Ba$, and three part system with $MO - M' - SiO_2$ with $M = Ca, Sr, Ba$ and $M' = Li, Mg, Al, Zn$. The two part silicate phosphates are promising for white light phosphors because of the Strong crystal field that causes teh emission to red shifting. The three part silicate phosphors how low emission of blue light and emits green light with UV excitation which is undesirable for white LEDS [8].

3.1.3 Nitride

Nitride based phosphors are a current interest due to strong thermal stability and strong crystal field effects caused by the electronegativity of N ions. There have been blue, green, and red emitting nitrate based phosphors reported [8]. The phosphor $LaAl(Si_5Al_1)N_9O_1 : Ce^{+3}$ has a tetrahedral crystal structure. When excited with 386 nm we can see a broad emission from 400 nm to 700 nm with a peak at 475 nm [8]. AlN doped with Eu^{+2} shows blue emission from 400 nm to 550 nm peaked at 465 nm. The excitation wavelength has absorption peaks at 230 nm, 289 nm, 342 nm, and 386 nm. The four excitation bands are caused by the crystal field splitting

of the $5d$ energy level of Eu^{+2}. However, the AlN crystal shows poor crystallinity [18].

3.2 Single Component lighting applications

The Current trend in research is to combine different color elements to form a single component white light source. This has been done by combining two dopants or codoping in a single inorganic crystal structure. With correct combination of dopants white light emitting diodes can be created. Some codoped phosphors show tunability of color by adjusting the concentration of the dopants. Furthermore, ET can use used in conjunction of with codoped phosphors to improve luminescence and color index. In this section we will highlight a few different cases of codoped inorganic phosphors.

First, we will discuss inorganic phosphors codoped with Eu^{2+}, and Mn^{2+}. Wu et all discuss a color-tunable $Ca_3Mg_3(PO_4)_4$ codoped with Eu^{+2} and Mn^{+2} [19]. As previously mentioned Eu^{2+} undergoes a UV light absorption and emits light in the blue region at around 450 nm. The transition metal Mn^{+2} absorbs light in the UV Blue region, and emits light in the the red-organish region. Mn^{2+} is a good source for a red light emitting component, but the transition of Mn^{2+} is forbidden. Through ET between Eu^{2+} and Mn^{2+} the emission of Mn^{2+} can be greatly improved. In $Ca_3Mg_3(PO_4)_4$ we can see a ET efficiency of 90% with a concentration of 0.6 of Mn^{2+} and Eu^{2+}. The ET type is classified as a dipole-quadrupole interaction with a

critical distance for ET to be 14.90 Å. As the concentration of Mn^{2+} is increased the emission wavelength is redshifted by the crystal field interaction from 596 nm to 661 nm.The color index of $Ca_3Mg_3(PO_4)_4$ is tunable from blue to white with increasing concentration of Mn [19].

Chen et al reported a color tunable $Ca_2Sr(PO_4)_2$ codoped with Eu^{2+} and Mn^{2+}. In this hosting material when doped with only Eu^{2+} we see a broad emission band from 400 nm to 700 nm. With increasng concentration of Mn the luminescence intensity of Eu^{2+} gradually decreases, and Mn^{2+} increase as typical with ET process. As the concentration of Mn is increases from 0.0 to 0.1 the color index changes from yellow-green to red. The ET type was identified as quadrupole-quadrupole interaction [20].

Guo et also created a tunable white light by codoping $Sr_3Y(PO_4)_3$ with Eu^{2+} and Mn^{2+}. For this hosting material we see broad emission of Eu^{+2} from 400 nm to 700 nm. Mn^{2+} shows emission peak at 600 nm for a low concentration of 0.005. As concentration increases the emission peak of Mn^{+2} redshifts to 632 nm. The hosting material codoped with Eu andMn shows color tunablity by changing the concentration from green to white. The ET type was identified as dipole-quadrupole type with a critical ET distance of 11.4 Å[21].

Chen et al reported white light emitting phosphor with the host material $Mg_2Al_4Si_5O_{18}$ codoped with Eu^{2+} and Mn^{2+}. The emission wavelength for Eu^{2+} is

found to be between 400 nm and 600 nm with the peak at 469 nm. The emission of Mn^{2+} has a broad emission peak from 400 nm to 800 nm centered at 600 nm. ET is observed between Eu^{2+} and Mn^{2+} with a dipole-quadrupole interaction. The critical concentration distance was found to be 23.65 Å. The luminescence of Mn^{2+} decreases after a concentration of 0.03 due to concentration quenching [22].

Orihashi et al reported codoped phosphor $CaZrO_3$ with Eu^{3+} and Bi^{3+}. The ET process occurs between Bi^{3+} and Eu^{3+}. In other words, Bi ion gives it energy to Eu. The ion Eu^{3+} has transition between$^5D_0 \rightarrow^7 F_J$ with $J = 0 - 6$ exhibiting several emission peaks above 500 nm. The transition are spin forbidden, so Eu^{3+} tend to have poor emission quality. The PL can be enhanced to 13 times by using Bi^{3+} as a donor through the ET process, and can serve as a red emitting phosphor [23].

3.3 Lighting Applications

Given the degree of research in this field along with the many reported phosphors the application is important to consider. Inorganic phosphors can be used for light signals such as street lights, and for LED with a blue chip. LEDs can operate with 10-20w power compared to incandescent lights which take 120W which is 93 % energy saving. Phosphors show a very long lifetime which make them great as a signal lighting source. Lastly LEDS based on phosphors are made up of arrays of light, so if one fails the

rest of the array will remain [8].

Chapter 4

Results and Discussion

We have two different hosting materials both codoped with Eu^{2+} and Mn^{2+}. To understand the effect of the hosting material on the emission and energy transfer between the activators we will use PL and TRPL methods to understand the interaction. A series of samples were synthesized from the Korean Institute (KRICT). For $Na(Sr, Ba)PO_4$ 5 samples were made with a constant concentration of $Mn_{0.05}$ and a varying concentration of Eu_x with $x = 0.01, 0.02, 0.05$. One sample if $Na(Sr, Ba)PO_4$ was doped with only $Eu_{0.05}$ and one sample was doped with only $Mn0.05$. For $Ba_2Mg(BO_3)_2$ 5 samples were made with varying concentrations of Mn^{2+}. One sample was doped only with $Eu^{2+}$for a given concentration of $Eu_0.2$. The other samples was codoped with $Eu_0.02$ and Mn_x for $x = 0.1, 0.15, 0.2, 0.3$.

4.1 PL Results

To measure the PL we use the experimental set up depicted in figure 2.3. However,instead of sending the emitted light through a monochromator we sent to light to a spectrometer to determine the emitted wavelengths.

For $Na(Sr, Ba)PO_4$ we can clearly see two separate emission peaks. The peak from 400 nm to 600 nm is from Eu^{2+}, and the peak from 525 nm to 700 nm is from Mn^{2+}. It is easy to confirm the emission wavelengths from the PL using the single doped phosphors. For ET to occur is is necessary for there to be overlap between the emission of the donor Eu^{2+} activator and the absorption of the the acceptor Mn^{2+}. Furthermore, we can see as the concentration of Eu^{2+} is increases the emission intensity of Mn^{2+} increases. This indicates ET from Eu^{2+} to Mn^{2+} 4.9.

For $Ba_2Mg(BO_3)_2$ we can see emission from single doped Eu^{2+} which emit light from 500 nm to 700 nm. This indicates the host $Ba_2Mg(BO_3)_2$ red shifts the emission of Eu^{2+}. The red shifting of Eu^{2+} has been studied by Diaz et al, and is caused by the crystal structure $Ba_2Mg(BO_3)_2$ [24]. After $Mn^{2+}$is added to the host the emission peak increase by 97 % with a concentration ratio $Eu_{0.2}/Mn_{0.1}$. Increasing the concentration of Mn^{2+} further we can see the luminescence intensity decrease by 60 % and decrease to roughly the same intensity of as a single doped $Ba_2Mg(BO_3)_2 : Eu^{2+}$ with a concentration of 0.2 and 0.3 of Mn. The reduction of

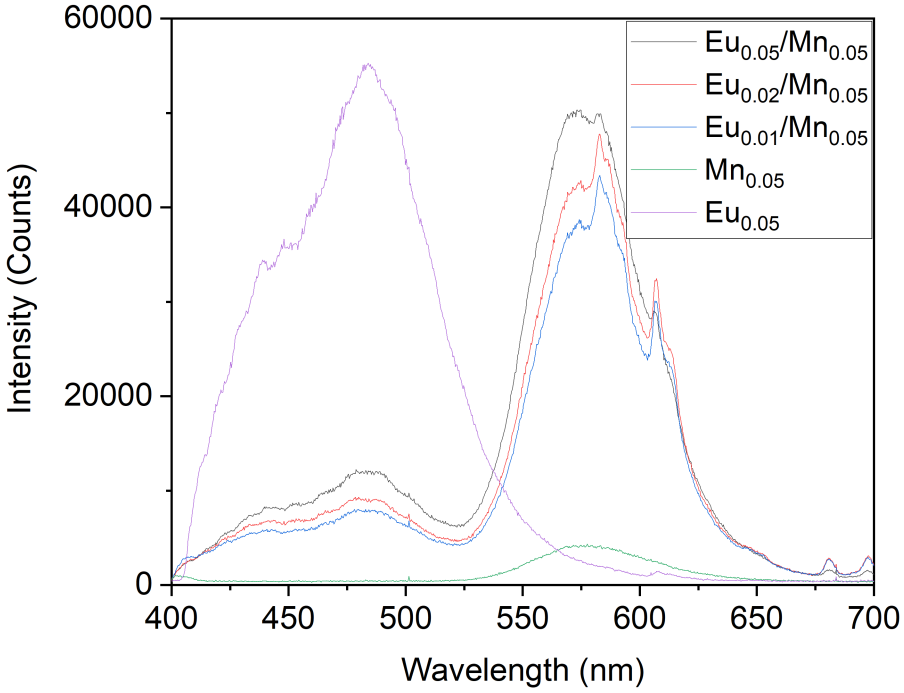

Figure 4.1: PL of Eu^{+2} and Mn^{+2} in $Na(Sr, Ba)PO4$ excited with 405 nm laser source

intensity with increasing concentration indicates that there concentration quenching present[2].

4.2 TRPL Results

The radiative lifetimes were determined using the set up in figure (2.3). For fluorescence lifetimes, the TCSPC method was used while phosphorescence lifetimes used an alternative method both described in chapter 2. The mean lifetime was determined

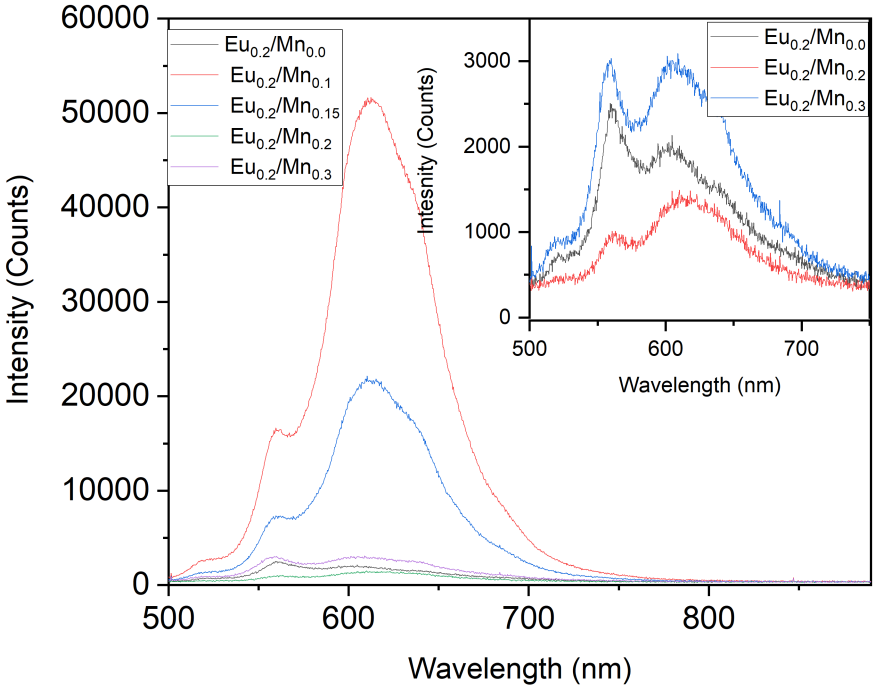

Figure 4.2: PL of Eu^{2+} and Mn^{2+} in $Ba_2Mg(BO_3)2$ excited using 405 nm laser source. The inset is an enlargement of the emission for concentration of Mn_x with $x = 0.0, 0.2, 0.3$

by fitting single exponential in the form

$$Ae^{\frac{-t}{\tau}}$$

with τ as mean lifetime, and A as the intensity in terms of counts. ET efficiency can be calculated by using $\eta = 1 - \frac{\tau_x}{\tau_0}$ [25] with τ_x as the lifetime with x as the concentration, and τ_0 as the lifetime without the acceptor. With the reduction of lifetime, we can find the efficiency of ET in each phosphor.

sample	Ratio Eu/Mn	Lifetime Eu^{2+}	Lifetime Mn^{2+}	RET %
sample 1	0.05/0.05	123 nm	46 ms	56 %
sample 2	0.05/0.02	125 ns	47 ms	57 %
sample 3	0.05/0.01	198 ns	46 ms	30 %
sample4	$Mn_{0.05}$	N/A	105 ms	N/A
sample 4	$Eu_{0.05}$	284 ns	N/A	N/A

Table 4.1
Fluorescent lifetime of Eu^{2+}, phosphorescent lifetime Mn^{2+}, and ET efficiency in $Na(Sr, Ba)PO_4$

For $Na(Sr, Ba)PO_4$ we see a reduction in the lifetime of Eu^{2+} with increasing concentration of Eu^{2+}. Efficiency of ET are shown in Table 4.1. There is 56 % ET efficiency after a Eu^{2+} concentration of $x = 0.02$, and there is no change in the lifetime or efficiency for Eu^{2+} for the concentrations of $Eu_{0.02}$ and $Eu_{0.05}$. We can compare the change in intensity of Eu^{2+} and Mn^{2+} for different concentrations of Eu^{2+}. We can see the emission of Eu^{2+} decreases to 40 % of the intensity compared to the intensity of Eu^{2+} without Mn^{2+} for $x = 0.01$, and saturates at around 45 % the relative intensity for $x = 0.02, 0.05$. For Mn^{2+} we compared the relative intensity for Mn^{2+} at its max for $x = 0.05$. We can see the emission Mn^{2+} increases by 88% with concentration of $x = 0.05$ compared to emission of Mn^{2+} without Eu^{2+}. This shows ET between Eu^{2+} and Mn^{2+}.

The emission peak of Eu^{2+} and Mn^{2+} are convoluted in $Ba_2Mg(BO_3)2$, so we cannot separate the lifetime measurements through spectral filtering. Instead we can separate the lifetimes by taking advantage of the fact that Eu^{2+} undergoes an

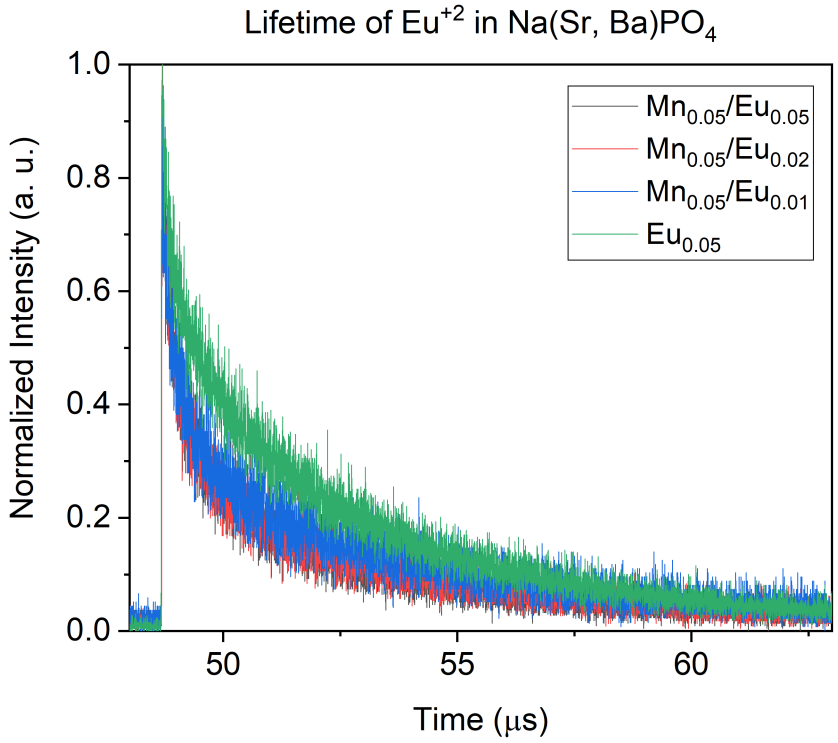

Figure 4.3: Lifetime of Eu^{2+} in $Na(Sr, Ba)PO_4$ measured using TCSPC for different concentration of Eu^{2+}

allowed radiative transition while Mn^{2+} has a forbidden transition. This means that Eu^{2+} will fluoresce at a fast time scale on the order of a few nanoseconds to a few microseconds while Mn^{2+} will decay at a time scale of a few hundred microseconds to a few milliseconds. To measure the lifetime of Eu^{2+} we measure the emission using the TCSPC method with a low rep rate to suppress the emission of Mn^{2+} since a low rep rate has a low average power output. This indicates that the decay curve measured using TCSPC is predominately from Eu^{2+}. Using this method we can see that the lifetime of purely doped Eu^{2+} has a lifetime 3.2 μs (table 4.2), and decreases with increasing concentration of Mn. The reduction of lifetime shows there

is a nonradiative ET process. More than likely we are seeing ET process between Eu^{2+} and Mn^{2+}.

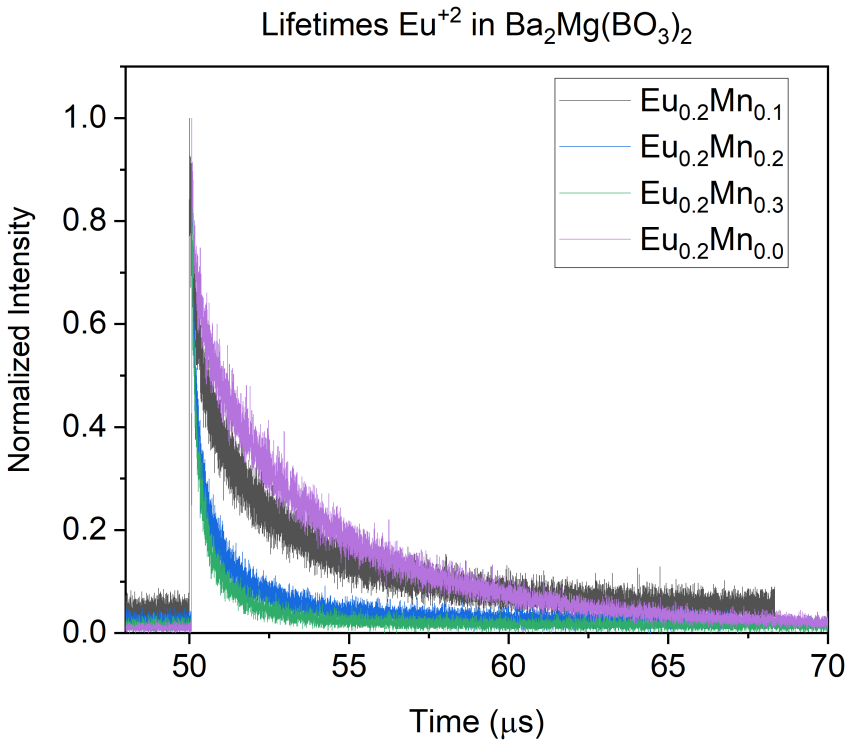

Figure 4.4: Lifetimes of Eu^{2+} in $Ba_2Mg(BO_3)_2$ for different concentrations of Mn

To measure the lifetime of Mn in both samples we switch from the HydraHarp 400 event counter to the MCS and add a optical chopper wheel to produce a periodic signal. From the lifetime measurements in $Na(Sr, Ba)PO_4$ we can see a reduction in the lifetime of Mn with Eu present. The lifetime is consistent for different concentrations of Eu 4.5.

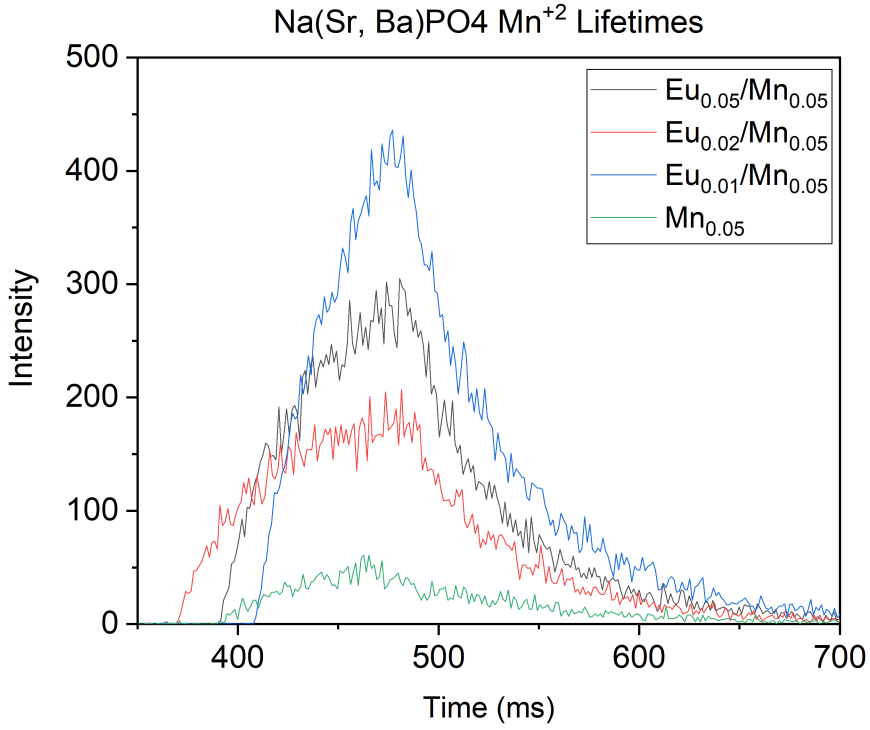

Figure 4.5: The decay curve of Mn^{2+} measured using a multiscalar for different concentration of Eu^{2+}

For the lifetime of Mn in $Ba_2Mg(BO_3)_2$ we can see a lifetime in the millisecond range. The lifetime also decreases for increasing concentrations of Mn indicating nonradiative interaction. This can indicate nonradiative interaction between $Mn - Mn$ [22] 4.4.

4.2.1 ET Critical distance

Besides the overlap between the absorption transition of the accepting activator and the emission of the donor activator, the distance between the two also effects the

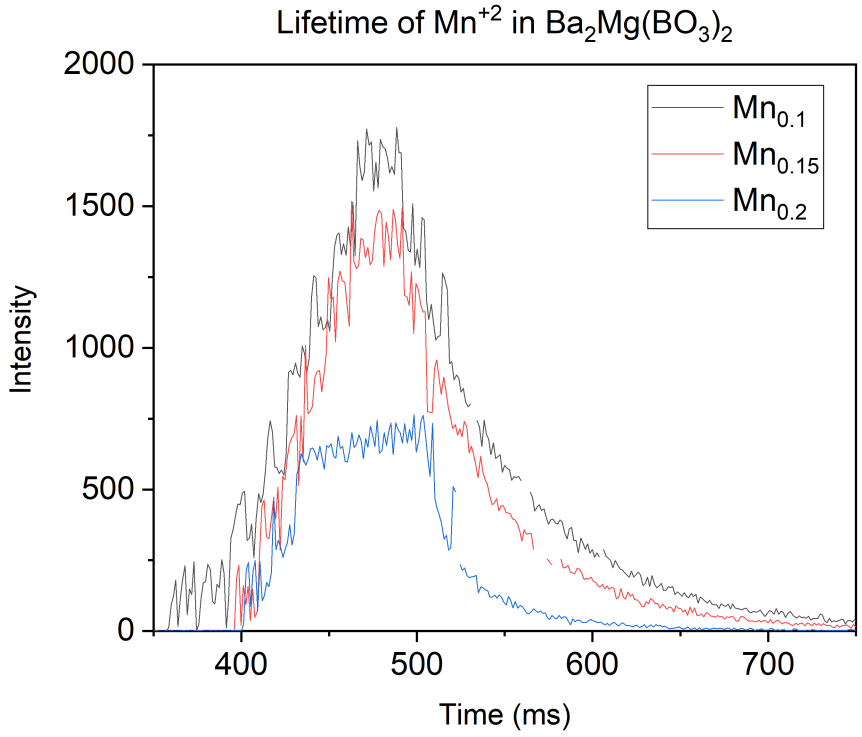

Figure 4.6: Decay curve for Mn^{2+} for different concentrations of Mn in the hosting material $Ba_2Mg(BO_3)_2$

ET. We can calculate the average distance R_{Eu-MN} between the donor Eu^{2+} and the acceptor Mn^{2+} using the formula introduced by Blasse [26] which is

$$R_{Eu-Mn} = 2[\frac{3V}{2\pi x_c N}]^{1/3} \tag{4.1}$$

with V as the unit cell volume, N as the Z ions, and x_C as the critical concentration. The critical concentration can be found when the emission intensity of the donor is reduced to half of the emission intensity of Eu^{2+} without the acceptor Mn^{2+}[22]. The unit cell volume and Z ions number were found for XRD for both $Na(Sr, Ba)PO_4$ and $Ba_2Mg(BO_3)_2$ [27], [28]. For $Na(Sr, Ba)PO_4$ $V = 187.32$ Å, $N = 2$, and $x_c = 0.01+$

sample	Ratio Eu/Mn	Lifetime Eu^{+2}	Lifetime Mn^{+2}	ET %
sample 1	0.2/0.00	3.2 μs	N/A	N/A
sample 2	0.2/0.1	1.6 μs	60ms	50%
sample 3	0.2/0.15	11.2 μs	51ms	63%
sample4	0.2/0.12	537ns	30ms	83%
sample 4	0.2/0.3	291ns	20ms	90%

Table 4.2
Fluorescent lifetime of Eu^{2+}, phosphorescent lifetime Mn^{2+}, and ET efficiency in $Ba_2Mg(BO_3)_2$

$0.05 = 0.06$ since the emission intensity is reduced to half with a concentration of 0.01 of Eu. This gives the critical ET distance of $R_{Eu-Mn} = 14.39$ Å. For $Ba_2Mg(BO_3)_2$ $V = 408.42$Å, $N = 3$, and $x_c = 0.2 + 0.1 = 0.3$. Because the emission peaks of Eu and Mn are convoluted, it is hard to discern the change in intensity. Since we can see a reduction in the lifetime of Eu^{2+} with the presence of a concentration of 0.1 of Mn^{2+} with an efficiency greater than 50 % along with the substantial increase in the luminescence intensity. It suffices to conclude that the critical concentration would be 0.1 of Mn. This gives the critical distance as $R_{Eu-Mn} = 9.53$ Å.

4.2.2 X-Ray Photoelectron Spectroscopy

The red emission present in $Ba_2Mg(BO_3)_2$ can come from Eu^{3+} ion. The emission from Eu^{3+} has three sharp emission peaks at 594 nm, 612 nm, and 624 nm and are associated with the $^5D_0 \rightarrow^7 F_i$ for $i = 1, 2, 3$, respectively [2], [29] . The PL for

$Ba_2Mg(BO_3)_2$ supports the emission is from Eu^{2+} since we see a broad emission peak instead of three spark peaks. The TRPL suggest the presence of Eu^{2+} since we are able to detect fluorescence lifetime in the microsecond range. The fluorescence lifetime measurements in the microsecond range also agree with the lifetimes reported by Diaz et al for Eu^{2+} [24]. However, to verify for the presence of Eu^{2+} compared to the Eu^{3+} ionization we utilize X-Ray photoelectric Spectroscopy (XPS). XPS is an excellent tool to obtain elemental composition of a substance. XPS essentially sends high energy x-rays towards a sample causing photoelectrons to be emitted. From the emission we can determine the binding energy which will respond to electron orbitals. For Eu^{3+} has $3d^{5/2}$ orbital which will give a binding energy of 1165 eV and 1135 eV. For Eu^{2+} has $3d^{3/2}$ which will give a binding energy of 1155 eV and 1135 eV [30]. From the XPS survey we can see three peaks at 1165 eV, 1135 eV, and 112 5eV. The peak at 1165 eV is from Eu^{3+} while the peak at 1135 eV is convoluted with Ba. We do see a peak at 1125 eV, but this is more than likely caused by a secondary electrons from Ba since the concentration of Ba is higher then Eu. The XPS was taken by the Applied Chemical and Morphological Analysis Laboratory (ACMAL) at Michigan Technology University. In conclusion, the XPS confirms the existence of Eu^{3+}, but does not show Eu^{2+} since we do not see a peak at 1155 eV. The XPS does not prove that Eu^{2+} is not present. Since the PL and TRPL data suggest the luminescence is form Eu^{2+} the sample $Ba_2Mg(BO_3)_2$ likely has both Eu^{2+} and Eu^{3+}.

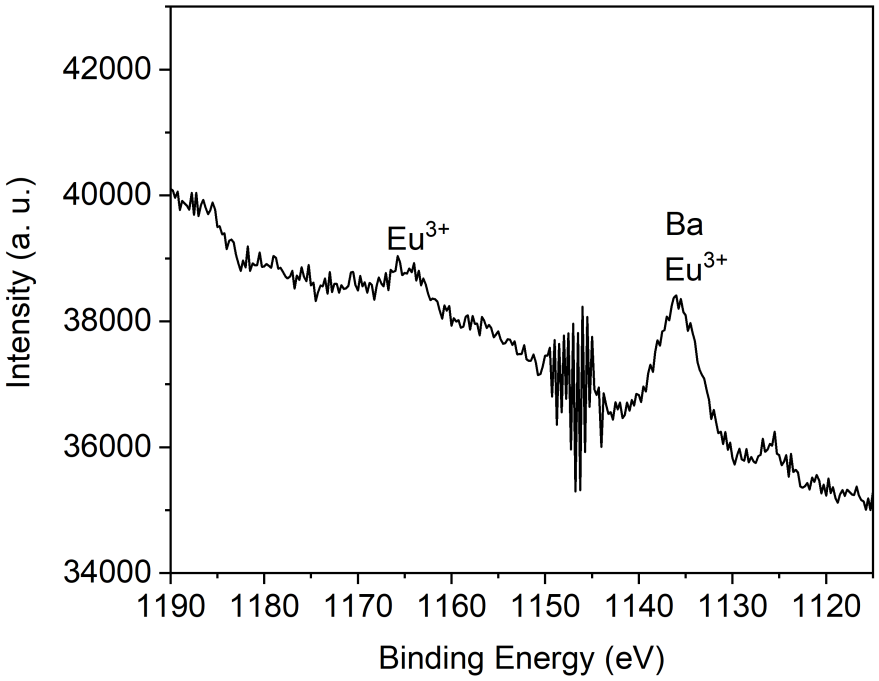

Figure 4.7: XPS data for $Ba_2Mg(BO_3)_2$ with peaks at 1165eV, 1135eV,a nd 1125eV. The peak1165eV is identified as Eu^{3+}, while 1135eV is Ba. Th Peak at 1125eV is likely a secondary electron from Ba

4.3 Discussion

The Phosphors $Na(Sr, Ba)PO_4$ and $Ba_2Mg(BO_3)_2$ are both codoped with Eu^{2+} and Mn^{2+}, but the ET process that occurs is quite different. The main different between the two phosphors is emission wavelength of the donor Eu^{2+} and the absorption band of Mn^{2+}. For $Na(Sr, Ba)PO_4$ the emission of Eu^{2+} is broad and peaked at 460 nm while in $Ba_2Mg(BO_3)_2$ the emission of Eu^{2+} is at 612 nm. For $Na(Sr, Ba)PO_4$ the relative intensity of Mn^{2+} increase to 80 % while ET efficiency increase to 30 %. With

more Eu added to $Na(Sr, Ba)PO_4$ the intensity and ET efficiency increases slightly (figure 4.9). In contrast, the relative intensity increases to 97 % when a concentration of $Mn_0.1$ is added to the host with an ET efficiency of 50 %. Furthermore, the ET efficiency continues to increase for increasing concentration of Mn. (figure 4.8). The data suggests that the ET is more efficient when there is substantial overlap between the absorption, and emission of the acceptor and donor. To say another way, ET is improved when a "resonance" condition is satisfied (figure 4.10).

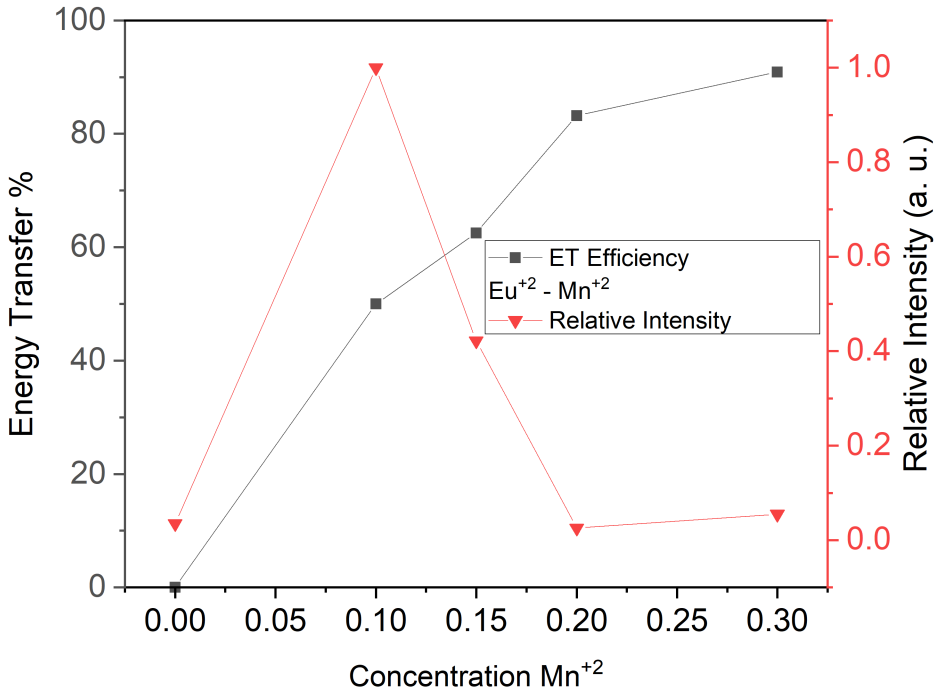

Figure 4.8: The RET efficiency compared to the relative intensity of Eu^{+2} and Mn^{+2}

Unfortunately even though the ET efficiency is improved in comparison to

$Na(Sr, Ba)PO_4$ the luminescence is none the less quenched with increasing concentration Mn. The reduction is lifetime of Mn^{2+} suggests an ET with $Mn - Mn$ interaction since the luminescence is being loss. More than likely the energy is being loss through a donor-killer interaction. In this process the ET occurs through a chain of several activators until it is transferred to a single activator which dissipates the energy. This particular activator is called a killer [2].

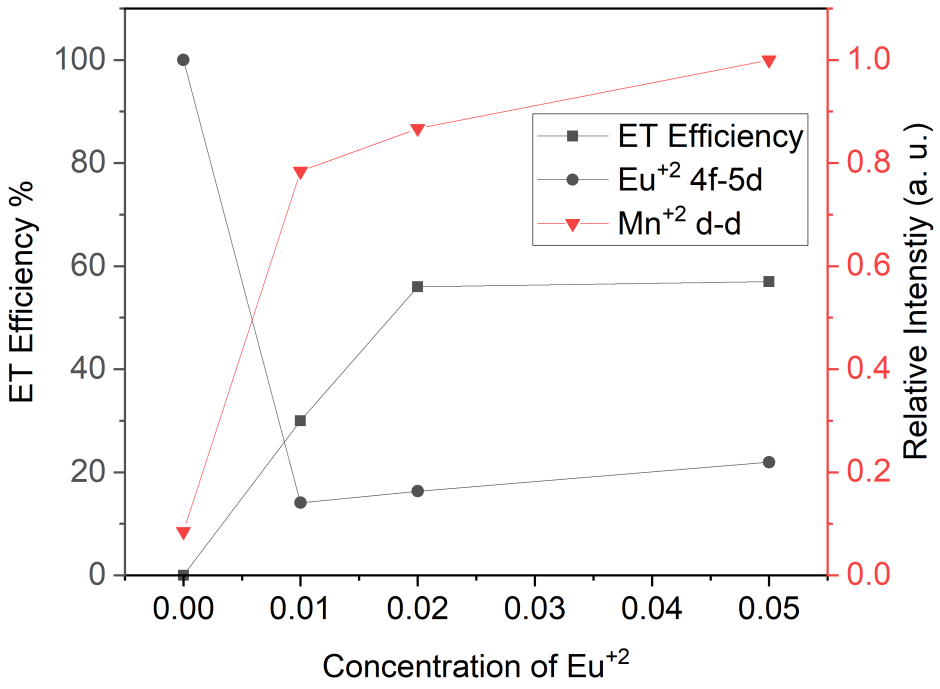

Figure 4.9: RET efficiency compared to the relative emission of Eu^{+2} and Mn^{+2}

Lastly the presence of Eu^{3+} in the host changes the ET transfer process, and is worth discussion. It is known that Mn^{2+} can transfer energy to Eu^{3+} increasing the luminescence [31],[32]. In addition, Eu^{2+} can sensitized Eu^{3+} improving the

luminescence. Since Eu^{2+},Eu^{3+}, and Mn^{2+} all have overlapping emission spectrum, the ET can occur between Eu^{3+}. However, as the concentration of Mn^{2+} increases the lifetime reduces with increasing concentration of Mn^{2+}. This means the concentration quenching is caused by Mn-Mn interaction. To draw any conclusions, about he interaction between Eu^{3+} we would need to keep the concentration of Mn constant while changing the concentration of Eu.

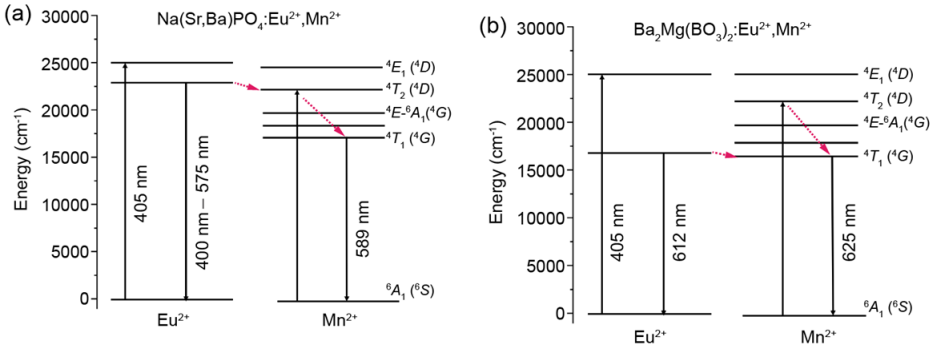

Figure 4.10: Energy Diagram for $Na(Sr, Ba)PO_4$ (a) and $Ba_2Mg(BO_3)_2$ (b). The dotted arrow indicates nonradiative process while the solid arrow indicate radiative process

Chapter 5

Conclusion

In conclusion, two series of the phosphors $Na(Sr, Ba)PO_4$ and $Ba_2Mg(BO_3)_2$ with varying concentration of Eu an Mn were produced. The luminescence properties were characterized with PL and TRPL measurements.

The PL shows the luminescence of the activators Eu^{2+} and Mn^{2+} in the two phosphors $Na(Sr, Ba)PO_4$ and $Ba_2Mg(BO_3)_2$. The phosphors were excited using a 405 nm laser and the emission was detected using an Oceanview spectrometer. We can see the emission of Eu^{2+} has a broad emission at 460 nm and Mn^{2+} has an emission at 580 nm. In comparison Eu^{2+} has emission at 612 nm and Mn^{2+} has emission at 625 nm. The stokes shift in the emission of Eu^{2+} in $Ba_2Mg(BO_3)_2$ is caused by crystal structure $Ba_2Mg(BO_3)_2$ [24]. We can observe crystal splitting in Mn^{2+} in $Ba_2Mg(BO_3)_2$ from the 625 nm emission of Mn^{2+} compared to the 580 nm

emission in $Na(Sr, Ba)PO_4$ [31].

The TRPL shows ET in both phosphors from Eu^{2+} to Mn^{2+}. The ET efficiency increases up to 56 % for $Na(Sr, Ba)PO_4$ and saturates at a concentration of $Eu_{0.02}$ (figure 4.9). In comparison, the ET efficiency continues to increase for $Ba_2Mg(BO_3)_2$ up to 97 % for an increasing concentration of Mn. The luminescence intensity increases by 80 % for an ET efficiency of 57 % for $Na(Sr, Ba)PO_4$.The max intensity for $Ba_2Mg(BO_3)_2$ occurs for a concentration of $Mn_{0.1}$ and an ET efficiency at 50 %. After the concentration increases above $Mn_{0.1}$ quenching occurs decreasing the luminescence intensity.

Comparing the two different host materials we can see that the luminescence is greater for $Ba_2Mg(BO_3)_2$ compared to $Na(Sr, Ba)PO_4$. Furthermore the ET is more efficient in $ba_2Mg(BO_3)_2$ than in $Na(Sr, Ba)PO_4$. Unfortunately, $Ba_2Mg(BO_3)_2$ suffers quenching hindering the luminescence. The improve efficiency in $Ba_2Mg(BO_3)_2$ can be attributed to the distant overlap between the energy level between Eu^{2+} and Mn^{2+} in $Ba_2Mg(BO_3)_2$ compared to the separation in $Na(Sr, Ba)PO_4$.

The significant of this find enables us to make more tailored phosphors for future lighting applications with ET. As shown the red emission of Mn^{2+} is greatly enhanced with Eu^{2+} when the emission is close to the emission transition of Mn^{2+}. We can further add another activator at a different wavelength in conjunction with

Eu^{2+} and Mn^{2+} which will emit blueish light to make a white light source with improved color index.

Bibliography

[1] Nakamura, S.; Mukai, T.; Senoh, M. *Applied Physics Letters* **1994**, *64*(13), 1687–1689.

[2] Solé, J.; Bausa, L.; Jaque, D. *An introduction to the optical spectroscopy of inorganic solids;* John Wiley & Sons, 2005.

[3] Optical properties of solids. Fox, M. **2002**.

[4] Einstein, A. *Phys. Z.* **1917**, *18*, 121–128.

[5] Planck, M. *Verh. Deut. Phys. Ges* **1900**, *2*, 237–245.

[6] Fox, M. *Quantum optics: an introduction*, Vol. 15; OUP Oxford, 2006.

[7] Shankar, R. *Principles of quantum mechanics;* Springer Science & Business Media, 2012.

[8] Xie, R.-J.; Li, Y. Q.; Hirosaki, N.; Yamamoto, H. *Nitride phosphors and solid-state lighting;* CRC Press, 2016.

[9] Novotny, L.; Hecht, B. *Principles of nano-optics;* Cambridge university press, 2012.

[10] George, N. C.; Denault, K. A.; Seshadri, R. *Annual Review of Materials Research* **2013**, *43*, 481–501.

[11] Jüstel, T.; Nikol, H.; Ronda, C. *Angewandte Chemie International Edition* **1998**, *37*(22), 3084–3103.

[12] Wahl, M. Time-corrleated single photon counting Technical report, PicoQuant, Picoquaint GmbH, Rudower Chaussee 29, 12489 Berlin, Germany.

[13] Eisaman, M. D.; Fan, J.; Migdall, A.; Polyakov, S. V. *Review of scientific instruments* **2011**, *82*(7), 071101.

[14] Becker, W. *Advanced time-correlated single photon counting techniques*, Vol. 81; Springer Science & Business Media, 2005.

[15] Scherz, P. *Practical electronics for inventors;* McGraw-Hill, Inc., 2006.

[16] Becker, W. *The Bh TCSPC Handbook;* Becker & Hickl, 2017.

[17] Sr430 multichannel scaler/averager operating manual and programming reference. System, S. R.; Standford Research System, Stanford Research Systems, Inc. 1290-C Reamwood Avenue Sunnyvale, California 94089, 1.6 ed., **2013**.

[18] Inoue, K.; Hirosaki, N.; Xie, R.-J.; Takeda, T. *The Journal of Physical Chemistry C* **2009**, *113*(21), 9392–9397.

[19] Wu, W.; Xia, Z. *RSC Advances* **2013**, *3*(17), 6051–6057.

[20] Chen, Y.; Li, Y.; Wang, J.; Wu, M.; Wang, C. *The Journal of Physical Chemistry C* **2014**, *118*(23), 12494–12499.

[21] Guo, N.; Huang, Y.; Yang, M.; Song, Y.; Zheng, Y.; You, H. *Physical Chemistry Chemical Physics* **2011**, *13*(33), 15077–15082.

[22] Chen, J.; Liu, Y.; Fang, M.; Huang, Z. *Inorganic chemistry* **2014**, *53*(21), 11396–11403.

[23] Orihashi, T.; Nakamura, T.; Adachi, S. *RSC Advances* **2016**, *6*(70), 66130–66139.

[24] Diaz, A.; Keszler, D. A. *Chemistry of materials* **1997**, *9*(10), 2071–2077.

[25] Paulose, P.; Jose, G.; Thomas, V.; Unnikrishnan, N.; Warrier, M. *Journal of Physics and Chemistry of Solids* **2003**, *64*(5), 841–846.

[26] Blasse, G. *Physics Letters A* **1968**, *28*(6), 444–445.

[27] Yun, Y. J.; Kim, J. K.; Ju, J. Y.; Choi, S. K.; Park, W. I.; Suh, J. Y.; Jung, H.-k.; Kim, Y.; Choi, S. *Physical Chemistry Chemical Physics* **2017**, *19*(18), 11111–11119.

[28] Kim, S. J.; Yun, Y. J.; Jung, H.-K.; Choi, S. *Optics letters* **2014**, *39*(2), 251–254.

[29] Xia, Z.; Zhuang, J.; Liao, L. *Inorganic chemistry* **2012**, *51*(13), 7202–7209.

[30] Briggs, D. *Surface and Interface Analysis* **1981**, *3*(4), v–v.

[31] Song, E.; Zhao, W.; Dou, X.; Zhu, Y.; Yi, S.; Min, H. *Journal of Luminescence* **2012**, *132*(6), 1462–1467.

[32] Zou, W.; Yang, Z. S.; Lü, M. K.; Gu, F.; Wang, S. F. *Displays* **2005**, *26*(4-5), 143–146.